SEP 7 1990

AEDC-TR-76-133

Cy 3

TESTS OF THE ONERA CALIBRATION MODELS IN THREE TRANSONIC WIND TUNNELS

PROPULSION WIND TUNNEL FACILITY
ARNOLD ENGINEERING DEVELOPMENT CENTER
AIR FORCE SYSTEMS COMMAND
ARNOLD AIR FORCE STATION, TENNESSEE 37389

November 1976

Final Report for Period April 1974 – May 1976

Approved for public release; distribution unlimited.

PROPERTY OF U.S. AIR FORCE
AEDC TECHNICAL LIBRARY

Prepared for

DIRECTORATE OF TECHNOLOGY (DY)
ARNOLD ENGINEERING DEVELOPMENT CENTER
ARNOLD AIR FORCE STATION, TENNESSEE 37389

PROPERTY OF U.S. AIR FORCE
AEDC TECHNICAL LIBRARY
ARNOLD AFB, TN 37389

NOTICES

When U. S. Government drawings specifications, or other data are used for any purpose other than a definitely related Government procurement operation, the Government thereby incurs no responsibility nor any obligation whatsoever, and the fact that the Government may have formulated, furnished, or in any way supplied the said drawings, specifications, or other data, is not to be regarded by implication or otherwise, or in any manner licensing the holder or any other person or corporation, or conveying any rights or permission to manufacture, use, or sell any patented invention that may in any way be related thereto.

Qualified users may obtain copies of this report from the Defense Documentation Center.

References to named commercial products in this report are not to be considered in any sense as an endorsement of the product by the United States Air Force or the Government.

This report has been reviewed by the Information Office (OI) and is releasable to the National Technical Information Service (NTIS). At NTIS, it will be available to the general public, including foreign nations.

APPROVAL STATEMENT

This technical report has been reviewed and is approved for publication.

FOR THE COMMANDER

ROSS G. ROEPKE
Research & Development
Division
Directorate of Technology

ROBERT O. DIETZ
Director of Technology

REPORT DOCUMENTATION PAGE		READ INSTRUCTIONS BEFORE COMPLETING FORM
1 REPORT NUMBER AEDC-TR-76-133	2 GOVT ACCESSION NO.	3 RECIPIENT'S CATALOG NUMBER
4 TITLE (and Subtitle) TESTS OF THE ONERA CALIBRATION MODELS IN THREE TRANSONIC WIND TUNNELS		5 TYPE OF REPORT & PERIOD COVERED Final Report - April 1974 - May 1976 6 PERFORMING ORG REPORT NUMBER
7 AUTHOR(s) T. W. Binion, Jr., ARO, Inc.		8 CONTRACT OR GRANT NUMBER(s)
9 PERFORMING ORGANIZATION NAME AND ADDRESS Arnold Engineering Development Center (DY) Air Force Systems Command Arnold Air Force Station, Tennessee 37389		10 PROGRAM ELEMENT, PROJECT, TASK AREA & WORK UNIT NUMBERS Program Element 65807F
11 CONTROLLING OFFICE NAME AND ADDRESS Arnold Engineering Development Center (DYFS) Arnold Air Force Station, Tennessee 37389		12 REPORT DATE November 1976 13 NUMBER OF PAGES 74
14 MONITORING AGENCY NAME & ADDRESS (if different from Controlling Office)		15 SECURITY CLASS (of this report) UNCLASSIFIED 15a DECLASSIFICATION/DOWNGRADING SCHEDULE N/A

16 DISTRIBUTION STATEMENT (of this Report)

Approved for public release; distribution unlimited.

17 DISTRIBUTION STATEMENT (of the abstract entered in Block 20, if different from Report)

18 SUPPLEMENTARY NOTES

Available in DDC

19 KEY WORDS (Continue on reverse side if necessary and identify by block number)

wind tunnel	models	Reynolds numbers
test methods	M3, M5, C5	interference (walls)
ONERA	transitions	
calibration	transonic flow	

20 ABSTRACT (Continue on reverse side if necessary and identify by block number)

A cooperative effort between the Office National d'Etudes et de Recherches Aérospatiales (ONERA); the National Aeronautic and Space Administration, Ames Research Center (NASA-ARC); and the Arnold Engineering Development Center (AEDC) was accomplished whereby two ONERA "standard" calibration models (M3 and M5) and an area equivalent body of revolution (C5) were tested in the NASA-ARC 11-ft and the AEDC 16-ft and 4-ft transonic wind tunnels.

DD FORM 1 JAN 73 1473 EDITION OF 1 NOV 65 IS OBSOLETE

20. ABSTRACT (Continued)

The tests were designed to provide an experimental data base for (1) the evaluation of theoretical or empirical wall-interference correction factors and (2) the establishment of guidelines to allow reasonable selection of wind tunnel to model size ratios in the transonic speed regime. The results showed that large effects of Reynolds number, tunnel flow quality, and small difference in model geometry preclude a determination of wall interference from the M3 and M5 model data. The primary cause of the data differences is a variation in the wing shock/separation patterns between the three tunnel tests. Even though the model forces may, in certain instances, agree from tunnel to tunnel, pressure distributions showed the agreement to be fortuitous. The C5 model data indicated subsonic theory underpredicts the required blockage correction by a factor of two to ten and, because the blockage interference effect changes sign along the model, simply correcting the Mach number will not compensate for the transonic interference.

PREFACE

The work reported herein was conducted by the Arnold Engineering Development Center (AEDC), Air Force System Command (AFSC), under Program Element 65807F. The results were obtained by ARO, Inc. (a subsidiary of Sverdrup & Parcel and Associates, Inc.), contract operator of AEDC, AFSC, Arnold Air Force Station, Tennessee, under ARO Project Nos. P32A-29A and P32A-COA. The author of this report was T. W. Binion, Jr., ARO, Inc. The data analysis was completed on April 26, 1976, and the manuscript (ARO Control No. ARO-PWT-TR-76-68) was submitted for publication on July 1, 1976.

CONTENTS

		Page
1.0	INTRODUCTION	7
2.0	APPARATUS	
	2.1 Test Facilities	8
	2.2 Experimental Models	9
	2.3 Instrumentation	10
3.0	PROCEDURE	
	3.1 Experimental Procedure	10
	3.2 Precision of Measurements	11
4.0	RESULTS AND DISCUSSION	
	4.1 Effect of Boundary-Layer Transition and Reynolds Number	12
	4.2 Comparison of Data from the Three Tunnels	14
5.0	CONCLUDING REMARKS	24
	REFERENCES	25

ILLUSTRATIONS

Figure		
1.	Location of the Model in the Tunnels	27
2.	Model Installations	30
3.	Model Dimensions	33
4.	Model Solid Blockage in Tunnel 4T	34
5.	M5 Pressure Orifice Locations	35
6.	Summary of Test Conditions	36
7.	Aerodynamic Coefficients on the M5 Model with Fixed and Free Transition at M_∞ = 0.84 and Various Reynolds Numbers	37
8.	Aerodynamic Coefficients on the M3 Model with Fixed and Free Transition at M_∞ = 0.84 and Various Reynolds Numbers	40

Figure		Page
9.	Effect of Reynolds Number on the ONERA Model Data in the Three Wind Tunnels	43
10.	Effect of Fixing Transition on the M5 Wing Pressure Distribution in Tunnel 16T, $M_\infty = 0.84$, $Re = 1.80 \times 10^6$	44
11.	Effect of Reynolds Number on the M5 Wing Pressure Distribution with Fixed Transition in Tunnel 16T, $M_\infty = 0.84$	44
12.	Comparison of Force and Moment Coefficients at $M_\infty = 0.7$ in Tunnels 16T, 11TWT, and 4T	45
13.	Pressure at x/c = 0.01 and Separation Pattern on the M5 Wing at $M_\infty = 0.7$ in Tunnels 16T and 4T	48
14.	Force and Moment Coefficients at $M_\infty = 0.84$ in Tunnels 16T, 11TWT, and 4T	49
15.	Selected M5 Wing Pressure Distributions at $M_\infty = 0.84$	52
16.	Force and Moment Coefficients at $M_\infty = 0.90$ in Tunnels 16T, 11TWT, and 4T	53
17.	M5 Wing Pressure Coefficients at x/c = 0.46 in Tunnels 16T and 4T, $M_\infty = 0.90$	56
18.	Representative M5 Wing Pressure Distribution at $M_\infty = 0.9$, $\alpha = 0.5$ deg	57
19.	Force and Moment Coefficients at $M_\infty = 0.95$ in Tunnels 16T, 11TWT, and 4T	58
20.	M5 Wing Pressure Distribution at $M_\infty = 0.95$, Zero Lift	61
21.	Representative M5 Wing Pressure Distribution at $M_\infty = 0.95$, $\alpha = -2$ deg	62
22.	Force and Moment Coefficients at $M_\infty = 1.0$ in Tunnels 16T, 11TWT, and 4T	63
23.	Representative M5 Wing Pressure Distribution at $M_\infty = 1.0$, $\alpha = 0.5$ deg	66

Figure		Page
24.	Pressure Distribution on the C5 Model in the Three Wind Tunnels	67
25.	Theoretical Blockage Interference for the C5 Model in Tunnel 4T, Q = 0.6	71
26.	Effect of Mach Numbers on Local Pressure Measurements in the Three Wind Tunnels, C5 Model	72
	NOMENCLATURE	73

1.0 INTRODUCTION

Although wind tunnel testing in the transonic speed range is more than 25 years old, there is still insufficient information, except for very elementary model shapes, to assess the effect of the tunnel boundaries on the aerodynamic phenomena under investigation. A program was initiated at the Office National d'Etudes et de Recherches Aérospatiales (ONERA) to construct a series of "standard models" for use in evaluating Reynolds Number and blockage effects in various wind tunnels. Tests of the same model in different wind tunnels and different scales of the same basic configuration in a given tunnel were designed to provide an experimental data base for (1) the evaluation of theoretical or empirical correction procedures and (2) the establishment or confirmation of guidelines to allow wind tunnel users to select model to wind tunnel size ratios to satisfy specific test objectives.

A cooperative effort between ONERA; the National Aeronautics and Space Administration (NASA), Ames Research Center (ARC); and the Arnold Engineering Development Center (AEDC) was initiated whereby tests of two of the "standard models" (M3 and M5) and one area equivalent body of revolution (C5) would be conducted in the NASA-ARC 11-ft Transonic Wind Tunnel (11TWT) and the AEDC Propulsion Wind Tunnel (16T) and Aerodynamic Wind Tunnel (4T). The tests were conducted at identical conditions, with the same instrumentation and support hardware, and were designed to serve several purposes. From a classical viewpoint, wall interference may be divided into blockage, downwash, buoyancy, and streamline curvature effects. Recent experiments, Ref. 1, have indicated the classical division is valid when the flow is subsonic everywhere but casts serious doubts on the classical concepts when there is supercritical flow over the model. Comparison of data from the M5 model which contained both force and pressure instrumentation from the various tunnels should confirm the results of Ref. 1. Comparison of the M3 and M5 force data with fixed and free transition

should indicate effects attributable to manufacturing differences, the test section environment, Reynolds number, and wall interference. Finally, the tests with the C5 model were designed to provide data to confirm the theoretical correction procedure of Ref. 2, and to determine if blockage corrections for a model could be computed from an area equivalent body of revolution. It was also intended that the data from Tunnels 16T and 11TWT serve as near-interference-free data for comparison with data obtained on the three models in smaller wind tunnels.

2.0 APPARATUS

2.1 TEST FACILITIES

2.1.1 Tunnel 16T

The AEDC Propulsion Wind Tunnel (16T) is a variable density, continuous-flow tunnel capable of being operated at Mach numbers from 0.3 to 1.6 with Reynolds number variations up to six million per foot. The test section is 16 ft square by 40 ft long and is enclosed by 60-deg inclined-hole perforated walls of fixed six-percent porosity. The general arrangement of the test section is shown in Fig. 1a.

2.1.2 Tunnel 11TWT

The NASA-ARC 11-ft Transonic Wind Tunnel (11TWT) is a variable density, continuous-flow tunnel capable of being operated at Mach numbers from 0.7 to 1.4 with Reynolds number variation up to ten million per foot. The test section is 11 ft square by 22 feet long. Each test section wall contains 12 baffled slots yielding a fixed 5.6-percent porosity. The general arrangement of the test section is shown in Fig. 1b.

2.1.3 Tunnel 4T

The AEDC Aerodynamic Wind Tunnel (4T) is a variable density, continuous-flow tunnel capable of being operated at Mach numbers from 0.2 to 1.3 at Reynolds numbers up to five million per foot. The test section is 4 ft square by 12.5 ft long and is equipped with 60-deg inclined-hole variable porosity (0 to 10-percent) walls. The general arrangement of the test section and wall geometry is shown in Fig. 1c.

2.2 EXPERIMENTAL MODELS

The family of ONERA models, shown installed in the wind tunnels in Fig. 2, is of a typical transonic transport configuration. The wing and tail airfoils have a "peaky" type symmetric cross section with a maximum thickness of 10.5 percent occurring at the 37.5-percent chord location. The wings have a 30-deg sweep, a 7.31 aspect ratio, a taper ratio of 0.3, and are at 4-deg incidence with respect to the fuselage. Both the wings and elevators have 3 deg of dihedral. The pertinent dimensions of the M3 and M5 models are shown in Fig 3. The C5 model is an area equivalent body of revolution of the M5 configuration. The solid blockage distribution of the models and sting supports in Tunnel 4T are shown in Fig. 4.

Each model was sting mounted on a six-component balance. Not only were the sting contours near the model identical in the three tunnels, the sting configurations were duplicates of those used in the ONERA S2MA wind tunnel. In addition to the balance, the M5 model contained three, 48-port, Scanivalves® which were used to measure the wing pressures at locations indicated in Fig. 5. The C5 model was instrumented with two longitudinal rows of pressure orifices located 90 deg apart.

2.3 INSTRUMENTATION

Forces and moments were measured on each model with internal strain-gage balances whose output was processed through facility analog to digital converters. Model pressures were measured with 15-psid (M5) and 25-psia (C5) strain-gage transducers using 48-port Scanivalves. Model attitude was measured with the facility system in each tunnel and with a damped-pendulum angle-of-attack sensor located at the first sting juncture (see Fig. 2). Each angular measurement was corrected for model deflection caused by the aerodynamic loads.

3.0 PROCEDURE

3.1 EXPERIMENTAL PROCEDURE

Tests with the M3 and M5 model were conducted with the boundary-layer transition location fixed and free, whereas data were obtained on the C5 model with fixed-transition only. The transition location was fixed with triple-sieved glass beads with diameters of 0.0051 ± 0.002 in. for the M5 and C5 models and 0.0025 ± 0.00002 in. for the M3 model at the 7-percent chord line on all airfoil surfaces and 2.3 percent of the fuselage length. Sublimation material was used in both Tunnels 11TWT and 16T to verify that the boundary-layer trip was effective and for the free-transition case to verify that the model surface was smooth enough to allow transition to occur naturally.

Data were obtained at a constant Reynolds number at Mach numbers from 0.6 to 1.0 and at several Reynolds numbers at Mach number 0.84. A summary of test conditions is presented in Fig. 6. The wall porosity in Tunnel 4T was varied from 1.5 to 7 percent as a test variable.

After the desired tunnel free-stream conditions were established, the model was positioned to discrete gravimetric angles of attack from -4.5 to 4.5 deg. In some instances, model dynamics forced termination of the pitch polars before 4.5 deg was reached. The model was then rolled 180 deg in Tunnels 16T and 11TWT and data were obtained at -4.5 to -2.0 deg to establish the tunnel flow angularity. In Tunnel 4T, the tunnel flow angularity was deduced by limited inverted tests. In each tunnel, the instrumentation readings were recorded by an online computer system which reduced the raw data to engineering units, computed pertinent parameters, and tabulated the results.

3.2 PRECISION OF MEASUREMENTS

Uncertainties (bands which include 95 percent of the calibration data) of the basic tunnel parameters (P_{t_∞} and M_∞) were estimated from repeat calibrations of the instrumentation and from the repeatability and uniformity of the test section flow during tunnel calibrations. Uncertainties in the instrumentation systems were estimated from repeat calibrations of the systems against secondary standards whose precisions are traceable to the National Bureau of Standards calibration equipment. The uncertainties are combined using the Taylor series method of error propagation to determine the precision of the reduced parameters as follows:

Parameter	Model		
	M3	M5	C5
ΔC_N, ΔC_L	±0.007	±0.005	-
ΔC_A, ΔC_D	±0.002	±0.002	-
ΔC_m	±0.005	±0.003	-
ΔC_p	-	±0.014	±0.014
$\Delta\alpha$	±0.1	±0.1	±0.1

4.0 RESULTS AND DISCUSSION

4.1 EFFECT OF BOUNDARY-LAYER TRANSITION AND REYNOLDS NUMBER

It is, in general, expected that data taken on the same model with free boundary-layer transition in different wind tunnels will not be the same because of differences in tunnel flow quality. One means of characterizing tunnel flow quality is through the concept of transition Reynolds number, Ref. 3. Dougherty and Steinle, Ref. 4, have shown the transition Reynolds number on a 10-deg cone to be quite different in Tunnels 16T, 11TWT, and 4T. In an effort to compensate for different effective Re in the three test facilities, transition was fixed by adhering glass beads at seven-percent chord to the wing and tail surfaces of the ONERA models. The bead size was established during the Tunnel 11TWT tests which were conducted first. The fact that transition did indeed occur at the trip location was verified by a sublimation technique in Tunnels 11TWT and 16T. In addition, the sublimination technique was used to assure that transition occurred naturally for the free-transition case in both tunnels.

Data obtained in Tunnels 16T, 11TWT, and 4T on the M3 and M5 models with both fixed and free transition at Mach number 0.84 and various Reynolds numbers are presented in Figs. 7 and 8. A cursory examination of the data is all that is required to establish the distressing fact that only in Tunnel 11TWT, and then only for C_N and C_D with fixed transition, are the data essentially independent of Reynolds number.

The magnitude of the Reynolds number dependency in the three tunnels may be more easily seen in Fig. 9 wherein the data are presented as lines of constant C_N as a function of Re. The symbol size in Fig. 9 is approximately equal to the data uncertainty. For

the free-transition case, α and C_A from Tunnels 16T and 11TWT approach an asymptotic value at about 2.5×10^6 Re. The asymptotic values are slightly different in each tunnel as one might expect because of variations in flow quality between the two facilities. In Tunnel 4T, where the data are more influenced by wall interference, only C_A approaches an asymptote. Whether this is caused by wall interference or the Tunnel 4T flow quality is, unfortunately, not discernible. However, it should be noted that a wall-interference investigation of a 2D supercritical airfoil, Ref. 5, indicated little variation of wall interference over an Re range from 7 to 30 million. Pitching moment is extremely Reynolds number dependent in each facility. The variations of C_m with Re is similar in the three tunnels but far from identical.

For the fixed-transition case, not only are the data more Reynolds number dependent than the free-transition case but the variation from tunnel to tunnel is greater. Pressure distributions obtained on the M5 model wing indicate the shock/separation pattern is significantly altered by fixing transition. Typical wing pressure distribution on the leeward surface from Tunnel 16T are shown in Fig. 10. Fixing transition causes a 0.1 $\bar{c}$ forward movement of the shock near the tip and midspan with a lesser movement at the root section for the case shown. Notice the trailing-edge boundary layer near midspan is separated with fixed transition and attached with free transition. A typical effect of Reynolds number on the wing pressure distribution with fixed transition is shown in Fig. 11 where the shock moves forward then aft at the midspan and inboard section as Reynolds number is increased. A significant reversal of the direction of the shock movement with increasing Re occurs only with fixed transition in Tunnel 16T. There is very little effect of either fixing transition or Reynolds number variation on the pressure distribution of the windward surface.

Returning to Fig. 9, careful comparison of the data obtained on the M5 model in Tunnel 4T reveals little effect of fixing transition at a constant Re (see also Fig. 7c). Even the pitching-moment data are

almost identical with fixed and free transition. Obviously, natural transition in Tunnel 4T occurred ahead of the trip location. Since the data are so sensitive to the state of the boundary layer, which in turn is apparently susceptible to the tunnel flow quality, it is impossible to precisely assess the effects of the wall interference on the M5 model by comparison of the data from one tunnel to the other. Furthermore, it is obvious by comparing the solid and open symbols in Fig. 9 that the M3 and M5 models are not sufficiently identical to allow a model-to-model comparison. The most serious discrepancy between the two models appears to be a difference in tail incidence causing different pitching-moment characteristics. It is rather ironic that the best agreement between the M3 and M5 model data occurs in Tunnel 4T where the models are subjected to the most wall interference.

4.2 COMPARISON OF DATA FROM THE THREE TUNNELS

It was the intent to use the ONERA model data from the large tunnels to infer the effects of wall interference in smaller facilities. However, because the data contain inseparable effects of tunnel flow quality, precise determination of wall-interference factors is impossible. Nevertheless, several methods were investigated to extract empirical influence factors, based on classical wall-interference theory, which would be indicative of the data differences from one tunnel to another. None of the attempts produced consistent results. Not only were the pseudo-interference factors dependent upon the aerodynamic coefficient being considered, they were also, at most Mach numbers, dependent upon the angle-of-attack range being considered. The analysis of Vaucheret and Vayssaire, Ref. 6, shows that empirical values of the wall porosity parameter, Q, determined from M5 model data at zero lift and a given Mach number were also dependent upon the aerodynamic coefficient being considered. The dependency in both cases results from attempting to apply classical, linear theoretical concepts to a highly nonlinear phenomena.

Unfortunately, state of the art wall-intereference theory, while perhaps providing useful guidelines, is, in general, inadequate with transonic flow over the model. Thus, the data obtained on the M3 and M5 models in Tunnels 16T, 11TWT, and 4T are compared in the suceeding analysis directly in terms of the aerodynamic coefficients rather than empirical interference parameters of doubtful utility. If it is assumed that the differences in Tunnels 16T and 11TWT are indicative of flow quality effects, the increments between Tunnels 16T and 4T data can at least provide a qualitative indication of the wall interference in Tunnel 4T. The symbol size used in the data figures approximates the data uncertainty in each parameter.

4.2.1 Determination of Model Incidence

As may be noted in subsequent figures, the data from both models show discrepancies in the zero lift angle of attack between the three tunnels. The values of α_0 were obtained in each of the tunnels by testing the model upright and inverted in a 4-deg angle range in the neighborhood of zero lift. In Tunnel 11TWT the inverted tests were accomplished by rolling the model with respect to the balance, whereas in Tunnels 16T and 4T the model and balance were rolled together. Data were taken in Tunnels 16T and 11TWT at each Mach number. However, in Tunnel 4T inverted data were taken only at selected Mach numbers and at only one porosity schedule. Thus, the small differences indicated between Tunnels 16T and 11TWT data reflect differences in technique as well as accuracy. However, as can be seen throughout the data the two techniques give results within the accuracy of the measurements. The α_0 data from Tunnel 4T, however, also reflect a lack of knowledge of the integrated tunnel flow angularities at porosities off the operating porosity schedule. For the purposes of this investigation, however, the small discrepancies in α_0 are of little consequence. The additional data gained in the time it would have required to take the inverted data far out weighs the worth of a third redundant measurement of α_0. The more important parameter to consider as an evaluation of wall interference is, of course, the lift curve slope.

4.2.2 Comparison of the M3 and M5 Model Data

Subsequent discussion in this section will consider the data taken in the three tunnels on the M3 and M5 configurations at representative Mach numbers in ascending order. Consider first the lift data taken at Mach number 0.7, Fig. 12a. The data from Tunnels 16T and 11TWT agree well except above 3 deg with the M3 model. Actually, Tunnels 11TWT and 4T lift data on the M3 agree better with each other than with Tunnel 16T. The values of $\partial C_L/\partial\alpha$ prior to stall are essentailly the same in the three tunnels for both models, which would imply no measurable wall interference. At angles of attack greater than about 0.5 deg the lift is greater in Tunnel 4T than in Tunnel 16T for both models. Wing pressure distributions taken on the M5 model indicate the flow becomes critical at an angle of attack of about -2 deg. While the terminal shock is at the same chord station in each tunnel, the minimum windward pressure coefficient is lower at all porosities in Tunnel 4T, -1.8 in Tunnel 4T compared with -1.55 in Tunnel 16T. At higher incidences a Type B1 separation* (after Pearcy et al., Ref. 7) occurs on the outboard portion of the wing in both tunnels. A shock-induced separation bubble is formed in each case at an angle of attack of about -1.5 deg. Divergence of the trailing-edge pressure occurs at α = 0.5 deg in Tunnel 4T and at about 1.0 deg in Tunnel 16T. However, once trailing-edge divergence occurs, the separated area on the outboard sections moves almost immediately to the wing leading edge in Tunnel 16T, whereas in Tunnel 4T separation does not reach the leading edge until α = 2.5 deg. Sketches of the phenomena inferred from the complete pressure distributions are presented in Fig. 13 along with the pressure at x/c = 0.01 on the leeward side of the wing versus angle of attack. The pressure distribution on the windward side was essentially identical

---

*The term Type B separation is used to designate a class of transonic flow in which trailing-edge spearation "plays a significant part in the overall development" of the wing separation pattern as opposed to Type A separations which are entirely shock induced.

in each case. Type B1 separation occurs at both sections 1 and 2. Section 3 appears to have a Type A separation in both tunnels with the separation not reaching the leading edge and with the rate of the bubble growth, ie, $dx/d\alpha$, almost identical in each case. The separation patterns in Tunnel 4T appear to be essentially independent of wall porosity. Since the size of the separated region on the M5 is smaller at a given incidence (>0.5 deg) in Tunnel 4T, the wing produces more lift than in Tunnel 16T. A similar phenomena of almost equal magnitude apparently occurs for the M3 since the lift increments (Tunnel 16T to Tunnel 4T) are essentially the same for the M3 and M5 models.

The agreement of the drag data at $M_\infty = 0.7$, Fig. 12b, between the three tunnels parallels that of the lift except for the M3 model in Tunnel 4T where the drag is consistently less than that in Tunnel 16T or Tunnel 11TWT throughout the Mach number range of the investigation. At least part of the discrepancy stems from a malfunction of the M3 base pressure instrumentation in Tunnel 4T. As a result, the drag comparisons presented for the M3 in Tunnel 4T are based on total drag rather than forebody drag. Nevertheless, even allowing for reasonable base pressures the axial force was still lower for the M3 in Tunnel 4T. The fact that the M5 drag is in relatively good agreement in the three facilities would tend to discredit arguments for a blockage-type effect causing the M3 differences. Thus since lift and pitching moment, to be discussed below, are in reasonable agreement it would appear that the skin friction was less on the M3 in Tunnel 4T than the other facilities.

The pitching moment, which for the ONERA models is much more sensitive to changes in the wing pressure distribution than either lift or drag, is presented in Fig. 12c. The data from the M5 in Tunnels 16T and 11TWT are in excellent agreement, whereas the data from Tunnel 4T reflect the effects of changes in the wing separation pattern. Tunnels 11TWT and 4T data for the M3 are, as with the lift, in much better agreement with each other than with the Tunnel 16T data.

The force and moment coefficient obtained in the three tunnels at M = 0.84 are presented in Fig. 14. The flow is supercritical at all angles of attack. The agreement between the data sets is very similar to that obtained at M = 0.7 except the divergence between the Tunnels 16T and 4T data begins at a lower angle of attack, i.e., -1 deg at M_∞ = 0.84 compared with 1.5 deg at M = 0.7. The pressure distribution on the M5 again indicates a Type B1 separation at station 1 in Tunnels 16T and 4T. The shock-induced separation begins at α = -2.0 deg in Tunnel 16T and -1.5 deg in Tunnel 4T with trailing-edge separation at about -1 deg in each case. But, as at M = 0.7, trailing-edge separation proceeds forward more slowly with increasing incidence in Tunnel 4T. Thus, because the extent of the trailing-edge separation is more forward, the terminal shock in Tunnel 16T is forward of that in Tunnel 4T. The pressure distributions at α = 0.5 deg, shown in Fig. 15a, are typical of that condition. At section 2, trailing-edge separation also occurs at about -1.0 deg in Tunnel 16T but does not occur at all in Tunnel 4T. As a result, the terminal shock at section 2 with α = -1.0 deg is also further forward in Tunnel 16T with correponding lift loss. An example is shown in Fig. 15b. However, the pressure distributions at section 2 for α = 3.5 deg are very similar in Tunnels 16T and 4T as shown in Fig. 15c. At section 3, the flow at the trailing edge is only slightly separated in Tunnel 16T which results in fairly good agreement of the data from the two tunnels even to relatively high angles of attack as indicated in Fig. 15d.

At each angle of attack the initial expansion over the leading edge of the wing is slightly greater in Tunnel 4T than in Tunnel 16T, Fig. 15. However, the effect of porosity in Tunnel 4T on all parameters is relatively minor. It is conceivable that the overexpansion in Tunnel 4T is the only effect attributable to wall interference. However, it is just as probable that the overexpansion is caused by transition moving to the leading edge in Tunnel 4T as discussed in Section 4.1, causing a thicker boundary layer than was experienced in Tunnel 16T.

At low angles of attack where the lift, drag, and the M5 wing pressure distributions from the two tunnels are in reasonable agreement, the pitching moment is not, for either model. Thus, it would appear that the flow field in the vicinity of the tail has been distorted in some manner also essentially independent of Tunnel 4T porosity.

As shown in Fig. 16, the agreement between Tunnels 16T and 11TWT data at $M_\infty = 0.9$ is essentially within the measurement accuracy except for two values of pitching moment on the M3 model. The lift data indicate Tunnel 4T is too closed at all porosities with both models. However, pressure data from the M5 wing again show that differences in the shock and separation patterns between Tunnels 16T and 4T are a major contributor to the data differences. Fig. 17 presents the pressure at $x/c = 0.46$ versus incidence, whereas Fig. 18 shows representative chordwise pressure distributions. Although the separation pattern near the wing tip at $\tau = 3$ percent in Tunnel 4T (Fig. 17a) is very similar to that in Tunnel 16T throughout the incidence range, the midspan pattern (Fig. 17b) is quite different at the higher angles as is the shock position at both stations (Figs. 18a and b) at positive angles of attack. The pressure at station 3 is independent of porosity in Tunnel 4T. However, there are small but significant differences between the measurements at station 3 in Tunnels 4T and 16T at negative incidence.

The data in Fig. 18 illustrates the flow over the forward portion of the wing is more expanded in Tunnel 4T than in Tunnel 16T. Local speeds are about 0.1 higher in Mach number in Tunnel 4T. However, based upon an examination of local pressure versus incidence, the flow in that region ($x/c = 0.2$) appears to be separated in Tunnel 16T and attached in Tunnel 4T. Thus, since the flow tends to stay attached, both in the neighborhood of the shocks and at the trailing edge, more in Tunnel 4T than in Tunnel 16T, it does not seem appropriate to attribute the difference in local velocity entirely to tunnel wall-interference perturbation velocities.

Note that porosity variations in Tunnel 4T affect the shock/separation locus on the M5 wing at $M_\infty = 0.9$, whereas at lower Mach numbers the pressure distributions were essentially independent of porosity. At section 1, Fig. 18, the terminal shock at $\tau = 3$ percent is forward of the shock in Tunnel 16T but is aft of the Tunnel 16T location at $\tau = 5$ and 7 percent. At sections 2 and 3, however, two other relationships are evident. However, as may be seen in Fig. 16, porosity changes have little effect on the total forces and moments with either model.

The force and moment data taken at $M_\infty = 0.95$ are presented in Fig. 19. Again, there is very good agreement between the data from Tunnels 16T and 11TWT for both models. In view of the differences seen at $M_\infty = 0.9$, it is surprising that the data for the M3 model from Tunnels 16T and 4T agree so well. Near zero lift, the lift and pitching moment for the M5 model in Tunnel 4T agree well with the two large tunnels. However, the wing pressure distributions for that condition, presented in Fig. 20, show the terminal shock in Tunnel 4T to be $0.09\bar{c}$ forward of the location in Tunnels 16T and 11TWT. The windward pressure distribution (not presented) are almost identical in each case. Obviously, the wing lift is less and the wing pitching moment is more positive in Tunnel 4T. Thus, it would appear that there is at $C_L=0$, $M_\infty = 0.95$, effects at the tail which exactly compensate for the discrepancies at the wing. At higher or lower angles of attack, the effects are not exactly offsetting but nevertheless appear to be opposite in sign in contrast to the disturbances present at lower Mach numbers. Apparently a similar phenomena also occurs with the M3 model since the agreement between C_m in Tunnels 16T and 4T is much better at $M_\infty = 0.95$ than the lower supercritical conditions.

The initial flow expansion over the forward portion of the wing for a given incidence at $M_\infty = 0.95$ is essentially the same in the three tunnels. Representative data are presented in Fig. 21. However, the terminal shock is more forward and the trailing-edge pressure is higher

in Tunnel 4T in every case. The difference between the shock location in Tunnels 16T and 4T is a function of span station. Thus, if wall interference is responsible for the shock displacement in Tunnel 4T, the perturbation velocities would appear to have a large spatial dependency.

The force and moment data obtained at $M_\infty = 1.0$ is presented in Fig. 22. It is astonishing that the lift and drag data on the M5 agree so well and appear to be independent of porosity in Tunnel 4T. While the lift data from the three tunnels on the M3 is also in excellent agreement, the M3 drag in Tunnel 4T is considerably less than was measured in either of the large facilities. The pitching-moment data on both models in Tunnel 4T are affected by disturbances probably in the region of the empennage. M5 wing pressure distributions in Tunnels 16T and 4T are essentially identical to the terminal shock position at all angles of attack. Typical distributions are shown in Fig. 23. The position of the terminal shock in Tunnel 4T is a function of porosity, moving downstream with increasing porosity. The terminal shock location at 7-percent porosity in Tunnel 4T at all angles of attack is almost identical to that in Tunnel 16T which accounts for relatively good agreement of the pitching moments for those two cases and poor agreement at the lower porosities.

4.2.3 Comparison of the C5 Model Data

Representative comparisons of the pressure distribution along the C5 model are presented in Fig. 24. The symbol size is approximately the same as the two-standard-deviation uncertainty of the data. The data from Tunnels 16T and 11TWT agree, except in rare instances, within the data accuracy at all Mach numbers. At $M_\infty = 0.8$ and below, the data from Tunnel 4T also agree (within the uncertainty band) with the data from the larger tunnels except near the rear of the model at $\tau = 7$ percent. As Mach number is increased the pressures in Tunnel 4T are,

in general, higher over the forward portion of the model and lower at the rear. Somewhat surprisingly, however, the flow over the bulge in the middle section which represents the wings is almost identical in all cases.

Theoretical calculations of blockage interference, using the method described in Ref. 2, are presented in Fig. 25 for the C5 model at various Mach numbers. The value of the porosity parameter, Q, of 0.6 is thought to be close to an average value for Tunnel 4T although, in reality, the wall boundary condition varies spatially with Mach number, porosity, and local boundary-layer parameters. The interference "trends" predicted by the subsonic theory are the same as observed in the experimental data. However, the magnitude of the interference pressure correction is less than the uncertainty of the experiment and varies with increasing Mach number from a factor of two to almost an order of magnitude smaller than the experimental data indicates. Similar results were obtained for a 2D lifting wing reported in Ref. 5. It should be noted that the experiment described in Ref. 2 used a model with a solid blockage and experimental technique almost identical to the C5 model. The experimental interferences measured in Ref. 2 were in good agreement with theory up to Mach numbers of 0.98. The magnitude of the interference calculations for the two cases was also very similar. However, the flow over the model in Ref. 2, a supercritical body of revolution, did not contain strong shock waves. In the present investigation a strong shock is present in the midportion of the C5 model where theory predicts, perhaps coincidentally, relatively little interference. The effects of the shock propagating both upstream and downstream could be the cause of the grossly underpredicted interference by the subsonic theory in the present case.

To illustrate the variation of the "blockage interference" with Mach number, the pressure at three axial stations on the C5 model is presented versus Mach number in Fig. 26. Also shown adjacent to the data

is the local pressure correction predicted by the subsonic theory but with an ordinate scale ten times that of the data. The data from Tunnels 16T and 11TWT are identical except in the region of the rapid expansion at $x/L = 0.536$ where the Tunnel 11TWT data are in closer agreement to the data from Tunnel 4T. It is suspected this discrepancy is caused by a small separation bubble forming in Tunnel 16T which did not occur in the other tunnels. If that is the case, then the Tunnel 4T data indicate unmeasurable interference throughout the Mach number range in the neighborhood of $x/L = 0.536$. The interferences upstream and downstream of the midsection, both measured and predicted, are of opposite sign which illustrates that simply incrementing the free-stream Mach number will not "correct" the data taken in the transonic range on models whose length-to-tunnel height ratio is not very small compared to unity.

It is interesting to note that the data on the forward portion of the model at $\tau = 7$ percent in Tunnel 4T agree well with the larger tunnel data throughout the Mach number range. In contrast, at the lower Mach numbers, the flow over the rear portion of the model is overexpanded at $\tau = 7$ percent in Tunnel 4T. It is possible the latter discrepancy could have been caused by operating the tunnel at other than optimum pressure ratio since the value used is an extrapolated value and not the result of a direct calibration at the conditions of the test. At the higher Mach number, however, the data from the rear portion of the model at $\tau = 7$ percent is essentially the same as that of the other porosities. Thus, it would appear that, in general, the better agreement obtained between Tunnels 16T and 4T in the M3 and M5 pitching-moment data at $\tau = 7$ percent at the higher Mach number is probably the result of a "more favorable" interaction of the wing flow field with the tunnel boundaries rather than a decrease in the blockage interference in the region of the empennage with increasing porosity.

5.0 CONCLUDING REMARKS

The large effects of Reynolds number, tunnel flow quality, and small differences in model geometry do not allow an assessment of wall interference to be made with the ONERA models. A primary cause of the data differences between the test of the M3 and M5 models in Tunnels 16T, 11TWT, and 4T is shown to be changes in the wing shock/separation patterns throughout the range of test variables. Both the M3 and M5 model data showed similar tunnel-to-tunnel variations except for the M3 drag which was consistantly lower in Tunnel 4T than in the larger facilities. However, as would be expected, the M3 model data from Tunnel 4T was closer to the large tunnel data because of the reduced blockage. Nevertheless, there was not a value of porosity in Tunnel 4T at any Mach number which resulted in a replication of the data from the larger facilities for either model. In fact, for a rare case in which the lift, drag, and pitching moment from Tunnel 4T at three values of porosity simultaneously agreed with Tunnels 16T and 11TWT values, the M5 wing pressure distributions showed the agreement to be fortuitous. Thus, the results of tests on the M3 and M5 models very dramatically show the necessity of evaluating the susceptibility of model data to Reynolds number and tunnel flow quality before attempting to lump all data discrepancies measured between two tunnel tests into a single category.

Tests to evaluate blockage effects of the C5 area equivalent body of revolution showed the variation of the experimental "interference" to agree well with the prediction of subsonic theory but to be larger in magnitude by a factor of two to ten as a function of Mach number. The C5 data also show that because the distribution of blockage interference changes sign along the length of the model, simply incrementing the free-stream Mach number will not compensate for the interference.

REFERENCES

1. Binion, T. W., Jr. "An Investigation of Three-Dimensional Wall Interference in a Variable Porosity Transonic Wind Tunnel." AEDC-TR-74-76 (AD787658), October 1974.

2. Binion, T. W., Jr. and Lo, C. F. "Application of Wall Corrections to Transonic Wind Tunnel Data." AIAA Paper 72-1009. Presented at the AIAA 7th Aerodynamic Testing Conference, Palo Alto, California, September 13-15, 1972.

3. Pate, S. R. and Schueler, C. J. "Radiated Aerodynamic Noise Effects on Boundary-Layer Transition in Supersonic and Hypersonic Wind Tunnels." AIAA Journal, Vol. 7, No. 3, March 1969, pp. 450-457.

4. Dougherty, N. S., Jr. and Steinle, Frank W., Jr. "Transition Reynolds Number Comparisons in Several Major Transonic Tunnels." AIAA Paper No. 74-627. Presented at the AIAA 8th Aerodynamic Testing Conference, Bethasda, Maryland, July 8-10, 1974.

5. Blackwell, James A., Jr. and Pounds, Gerald A. "Wind Tunnel Wall Interference Effects on a Supercritical Airfoil at Transonic Speeds." Paper Presented at the AIAA 9th Aerodynamic Testing Conference, Arlington, Texas, June 7-9, 1976.

6. Vaucheret, Xavier and Vayssaire, Jean-Charles. "Corrections De Parois En Ecoulement Tridimensionnel Transsonique Dans Des Veines A Parois Ventilees." Symposium on Wind Tunnel Design and Testing Techniques, October 6-8, 1975, London, England. AGARD Conference Proceedings No. 174.

7. Pearcey, H. H., Osborne, J., and Haines, A. B. "The Interaction Between Local Effects at the Shock and Rear Separation - A Source of Significant Scale Effects in Wind Tunnel Tests on Airfoils and Wings." Proceedings of the AGARD Conference on Transonic Aerodynamics, AGARD-CP-35, September 1968.

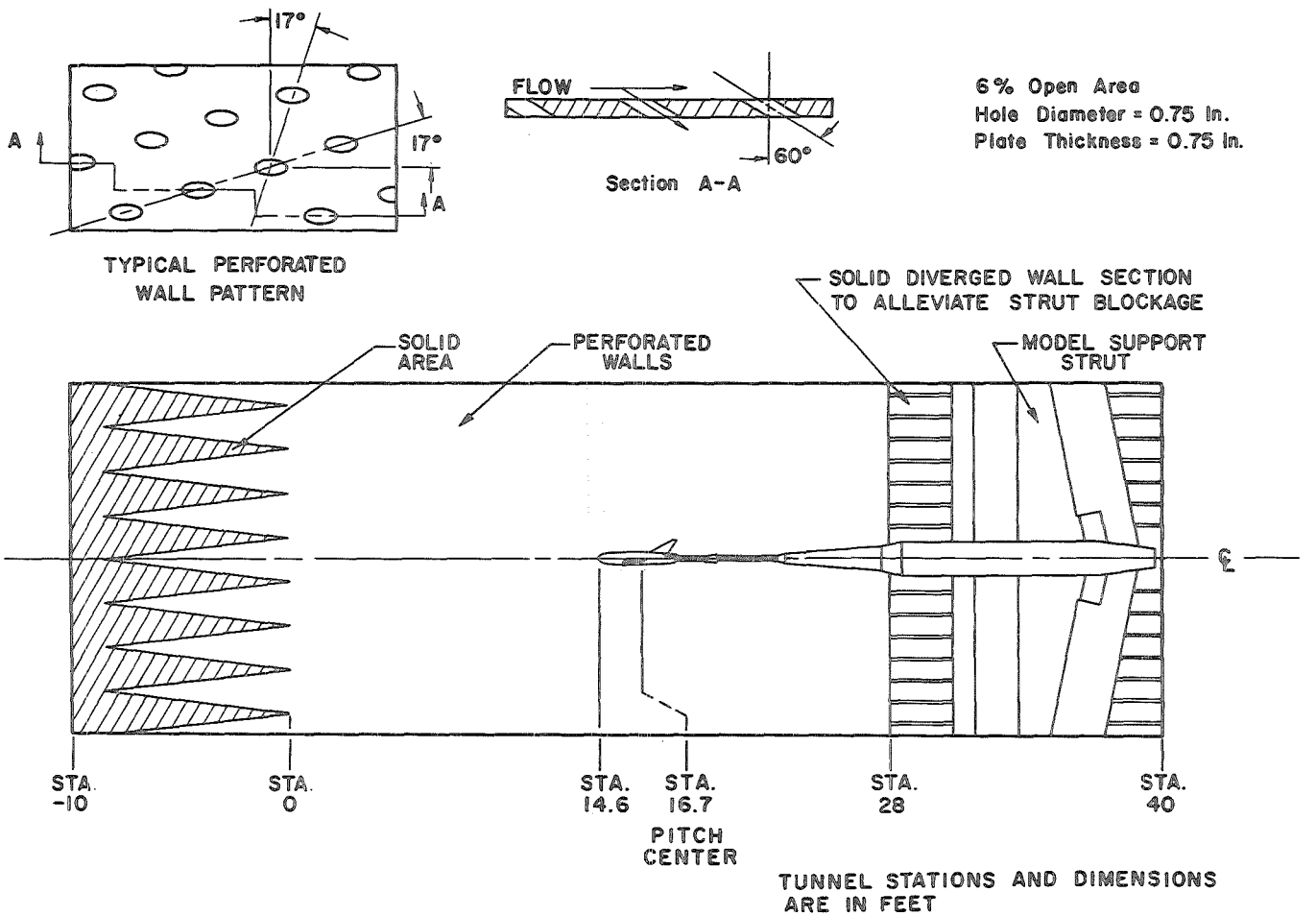

a. Tunnel 16T

Figure 1. Location of the model in the tunnels.

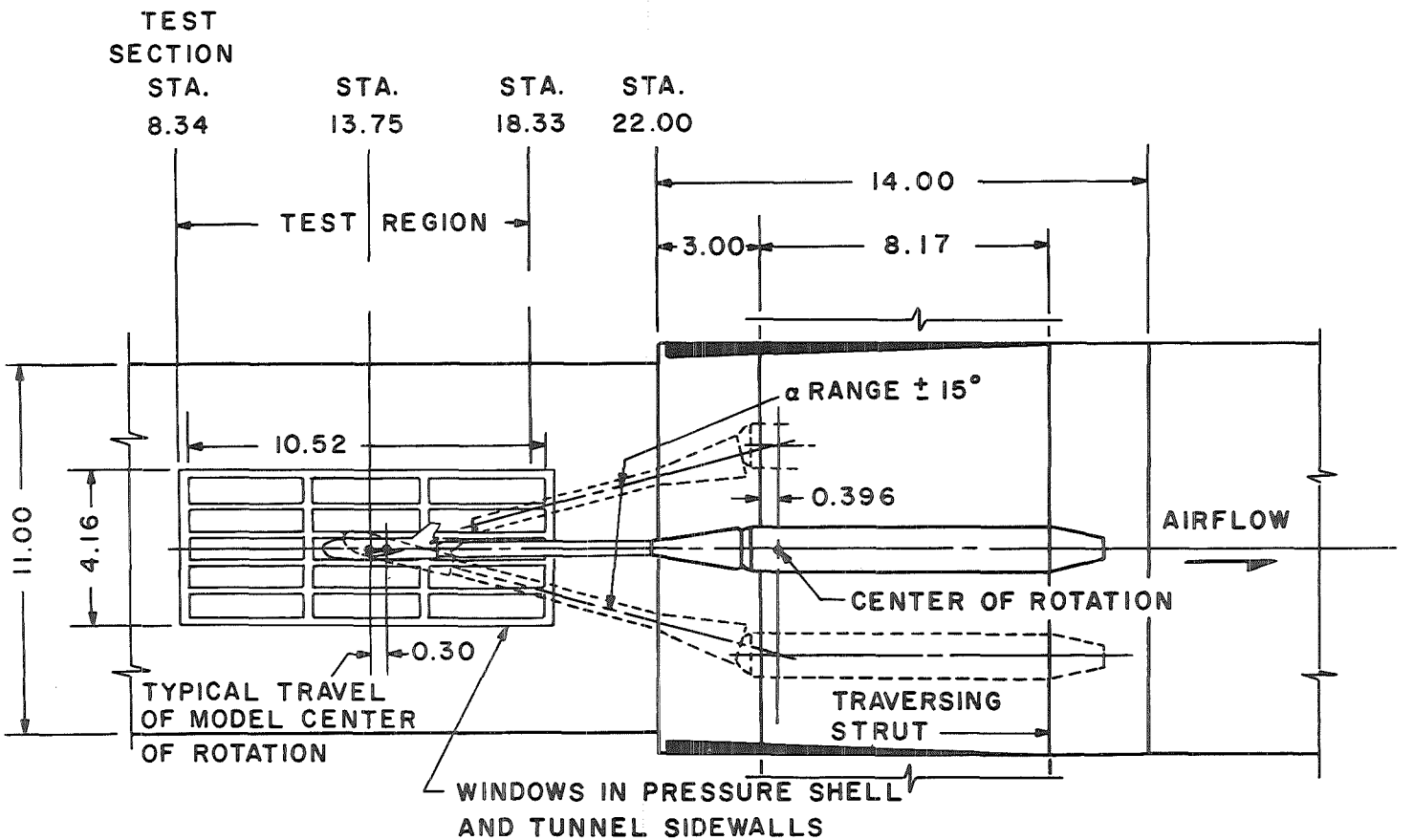

b. Tunnel 11TWT
Figure 1. Continued.

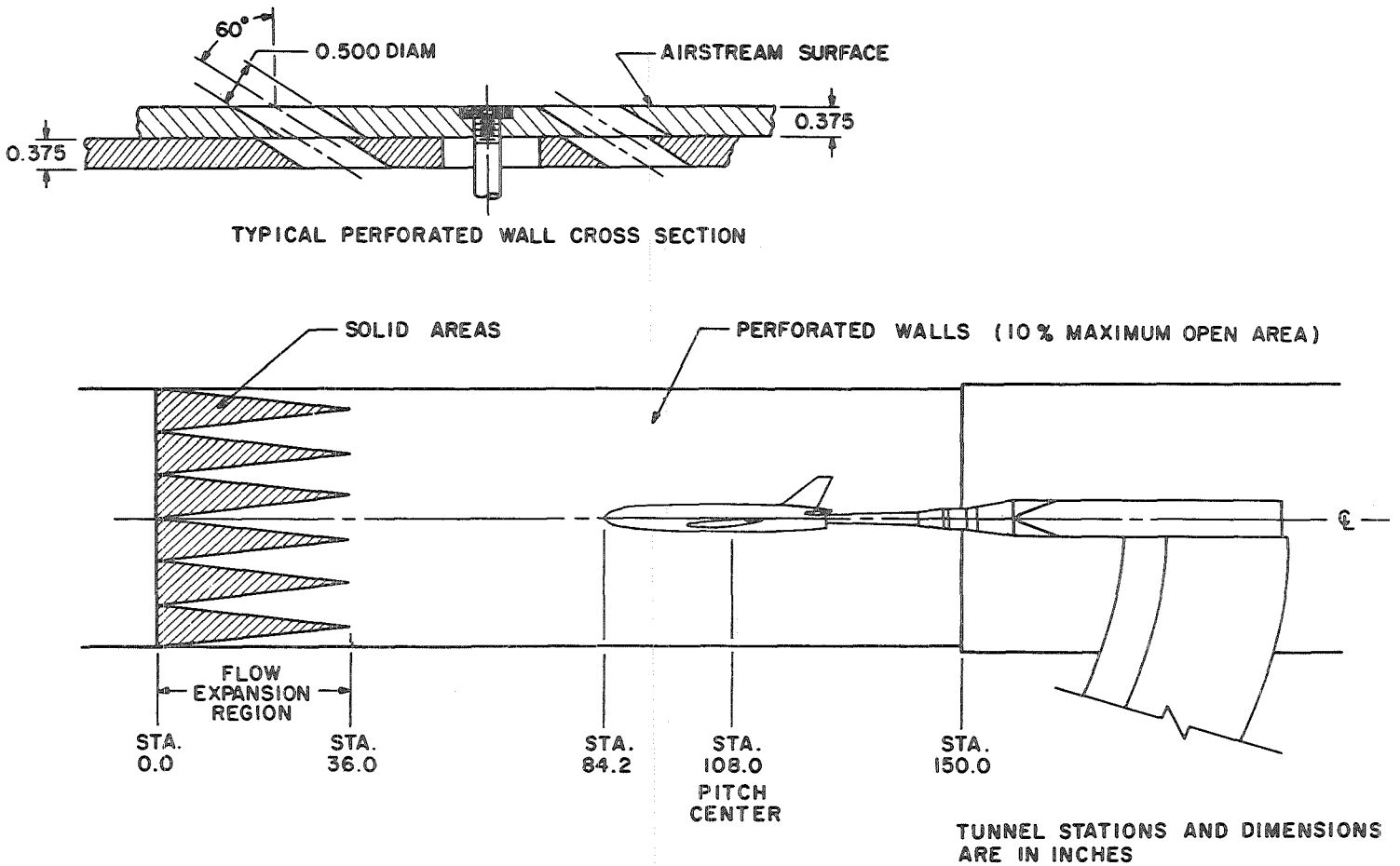

c. Tunnel 4T
Figure 1. Concluded.

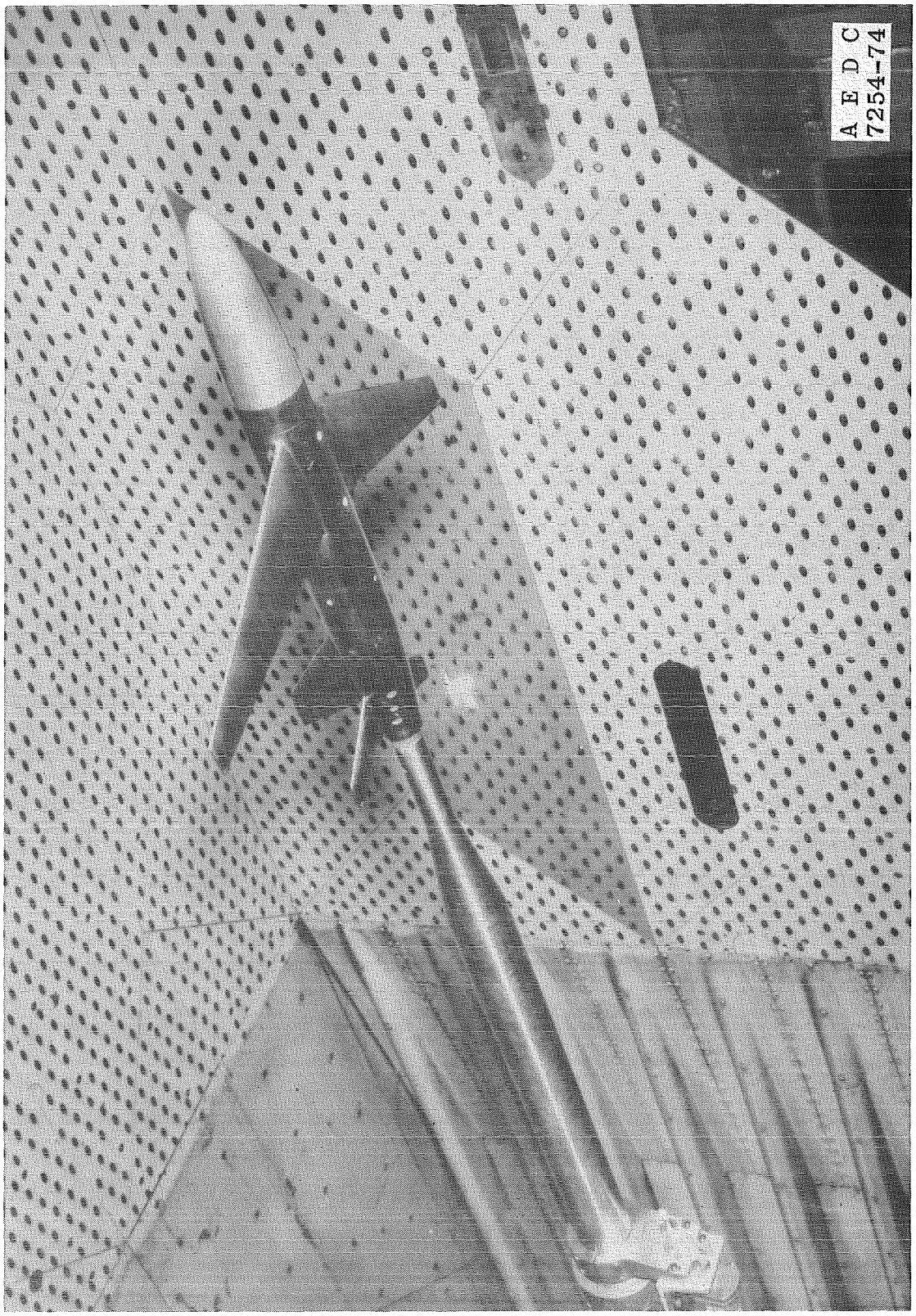

a. M3 model in Tunnel 16T
Figure 2. Model installations.

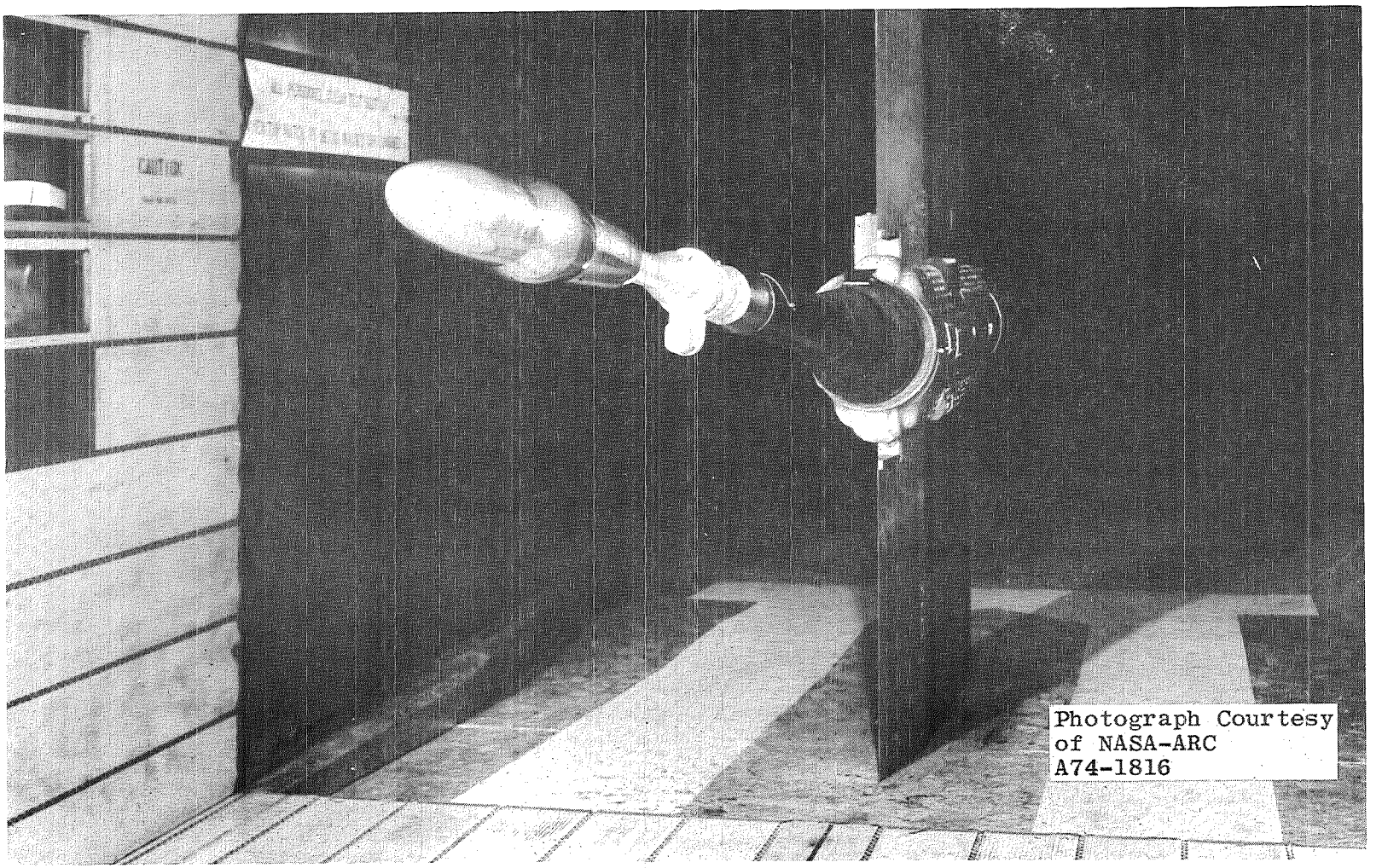

b. C5 model in Tunnel 11TWT
Figure 2. Continued.

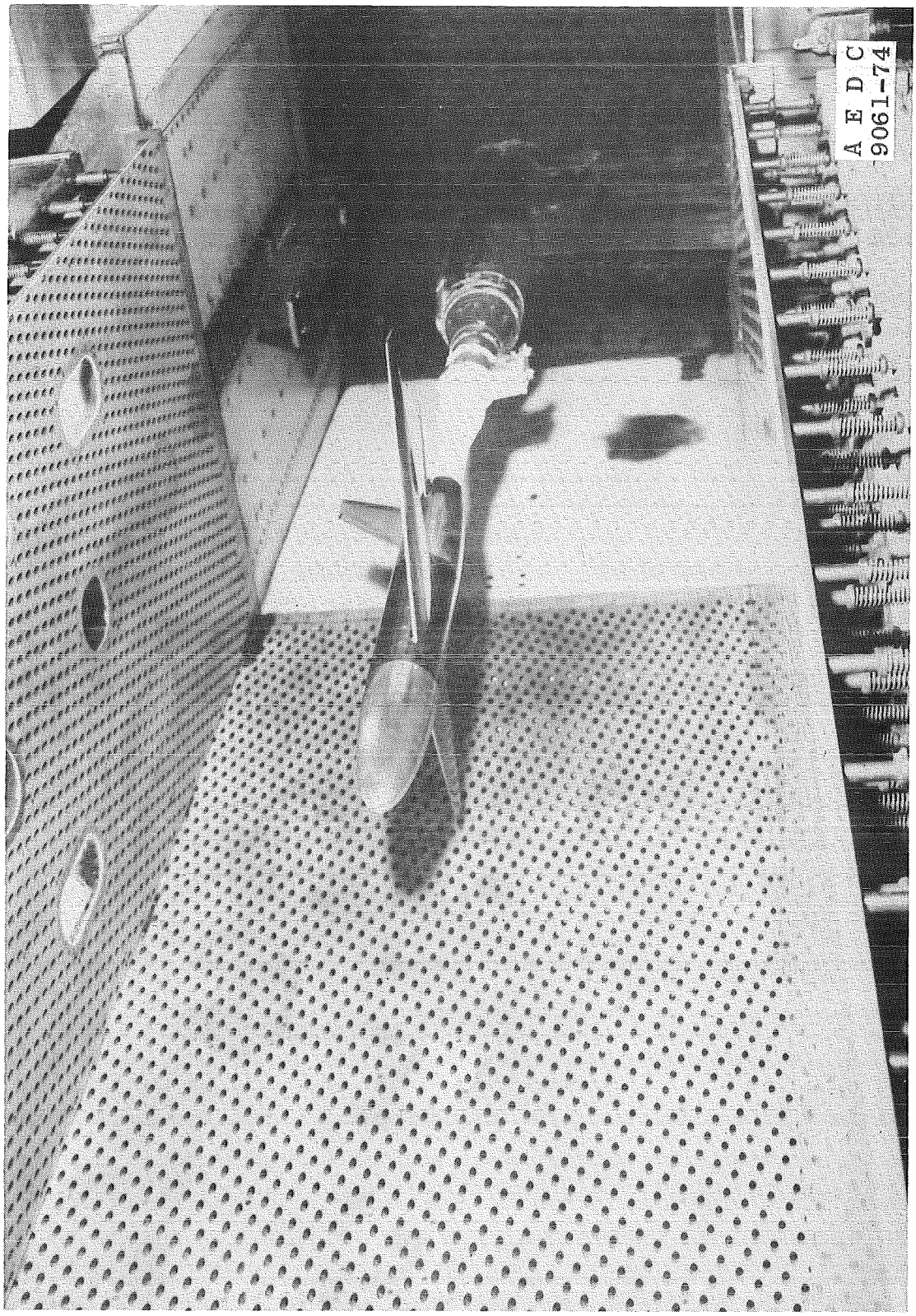

c. M5 model in Tunnel 4T
Figure 2. Concluded.

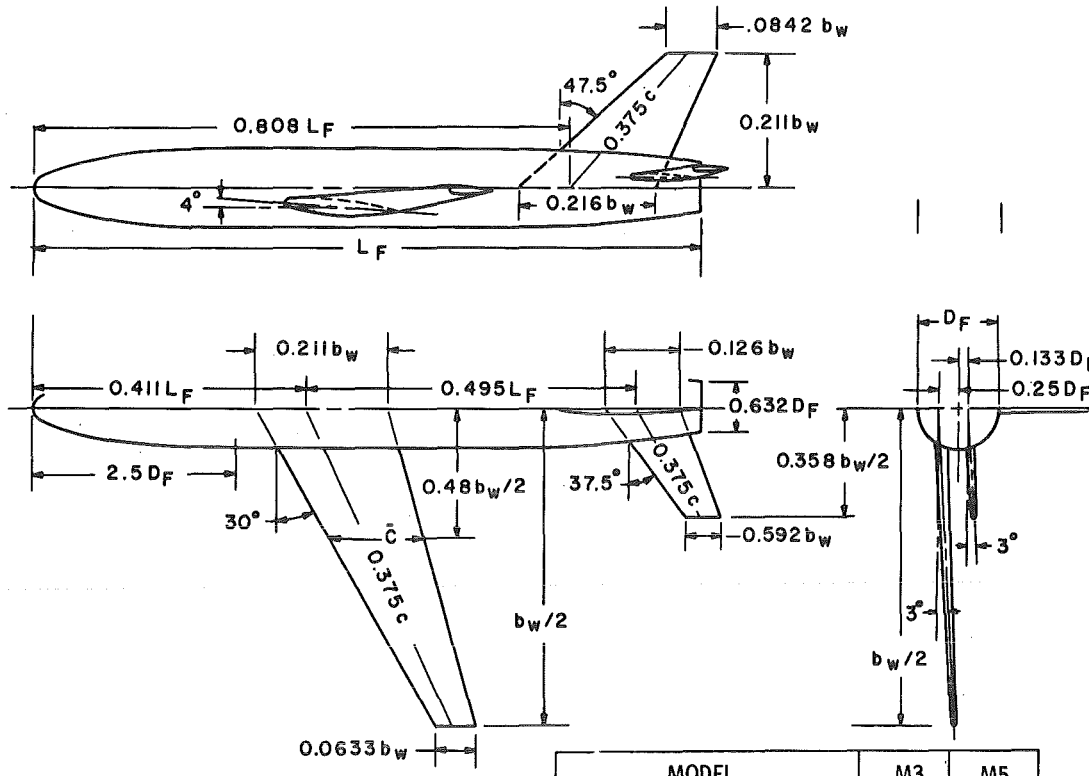

MODEL	M3	M5
Wing span, b_W (m)	0.474	0.982
Ref. chord, c (m)	0.066	0.137
Ref. surf, S (m^2)	0.031	0.132
Fus. length, L_F (m)	0.511	1.058
Fus. diam, D_F (m)	0.060	0.124
Max. cross section, (m^2)	0.0043	0.0183

Figure 3. Model dimensions.

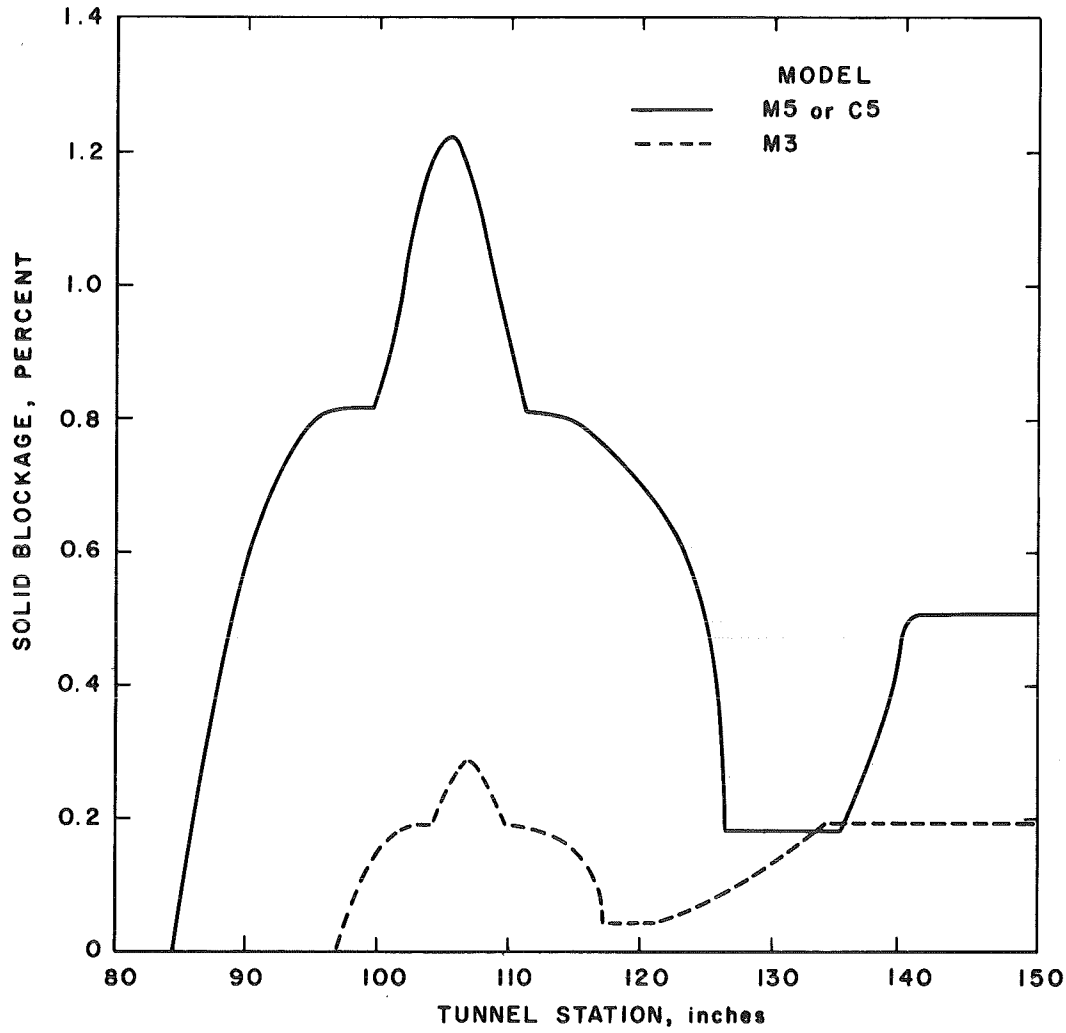

Figure 4. Model solid blockage in Tunnel 4T.

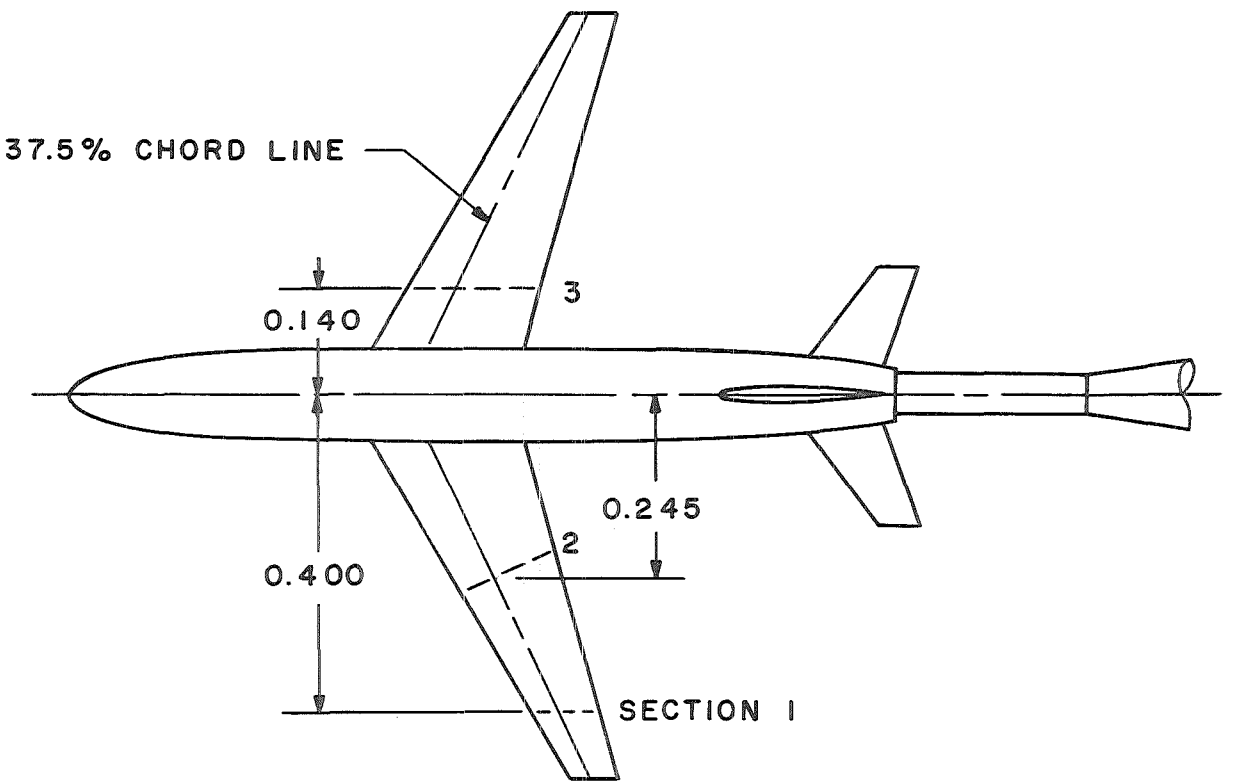

ALL DIMENSIONS IN METERS

Figure 5. M5 pressure orifice locations.

□ AEDC 16T
○ AEDC 4T
△ ARC 11TWT

OPEN SYMBOLS - FREE TRANSITION
SOLID SYMBOLS - FIXED TRANSITION
(MACH NO. WITHIN 0.01, REYNOLDS NO'S. WITHIN 10%)

ONERA MODEL CORRELATION STUDY—AVAILABILITY OF COMPARATIVE DATA

M5 MODEL

MACH NO. / REYNOLDS NO (unit 1/ft.)	0.60	0.70	0.80	0.84	0.87	0.90	0.925	0.95	0.97	0.98	0.99	1.00
1.55×10^6				□○ ■●								
2.27				□○△ ■●▲								
3.80				□○△ ■●▲								
4.00	■●▲	■●▲	■●▲	□○△ ■●▲	■●▲	■●▲	■●▲	■●▲	■●▲	■●▲	■●▲	■●▲
4.94				□○△ ■●▲								
5.87				□○△ ■●▲								
6.72				△ ▲								
8.00				△ ▲								

M3 MODEL

1.55×10^6				□○ ■●								
2.27				□○△ ■●								
3.80				□○ ■●								
4.00	■●	■●	■●	□○△ ■●▲	■●	■●	■●	■●	■●	■●	■●	■●
4.94	▲	▲	▲	□○△ ■●▲	▲	▲	▲	▲	▲	▲	▲	▲
5.87				□○△ ■●▲								
6.72				△								
8.00	▲	▲	▲	△ ▲	▲	▲	▲	▲	▲	▲	▲	▲

C5 MODEL

4.00	■●▲	■●▲	■●▲	■●▲	■●▲	■●▲	■●▲	■●▲	■●▲	■●▲	■●▲	■●▲

Figure 6. Summary of test conditions.

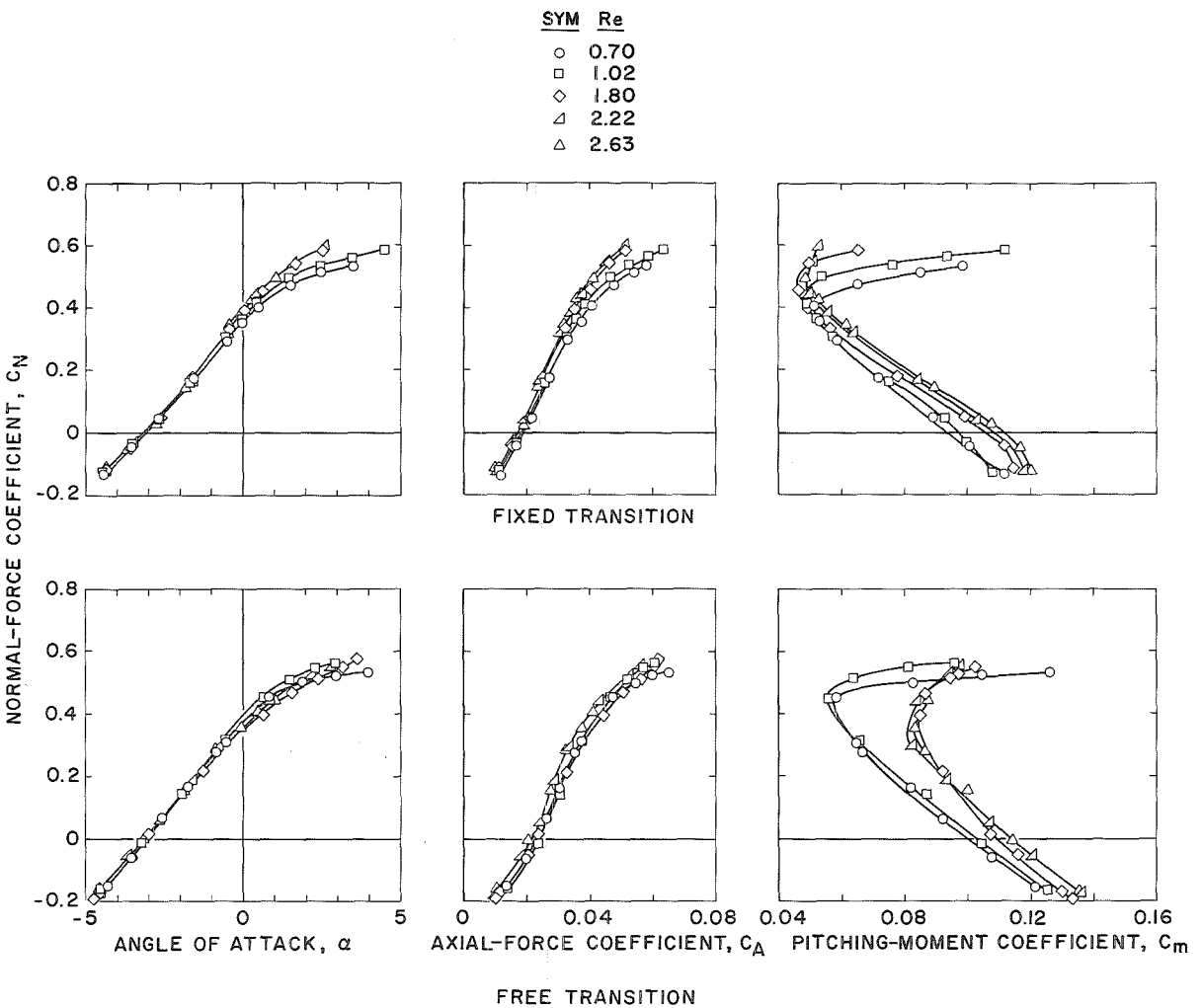

a. Tunnel 16T

Figure 7. Aerodynamic coefficients on the M5 model with fixed and free transition at M_∞ = 0.84 and various Reynolds numbers.

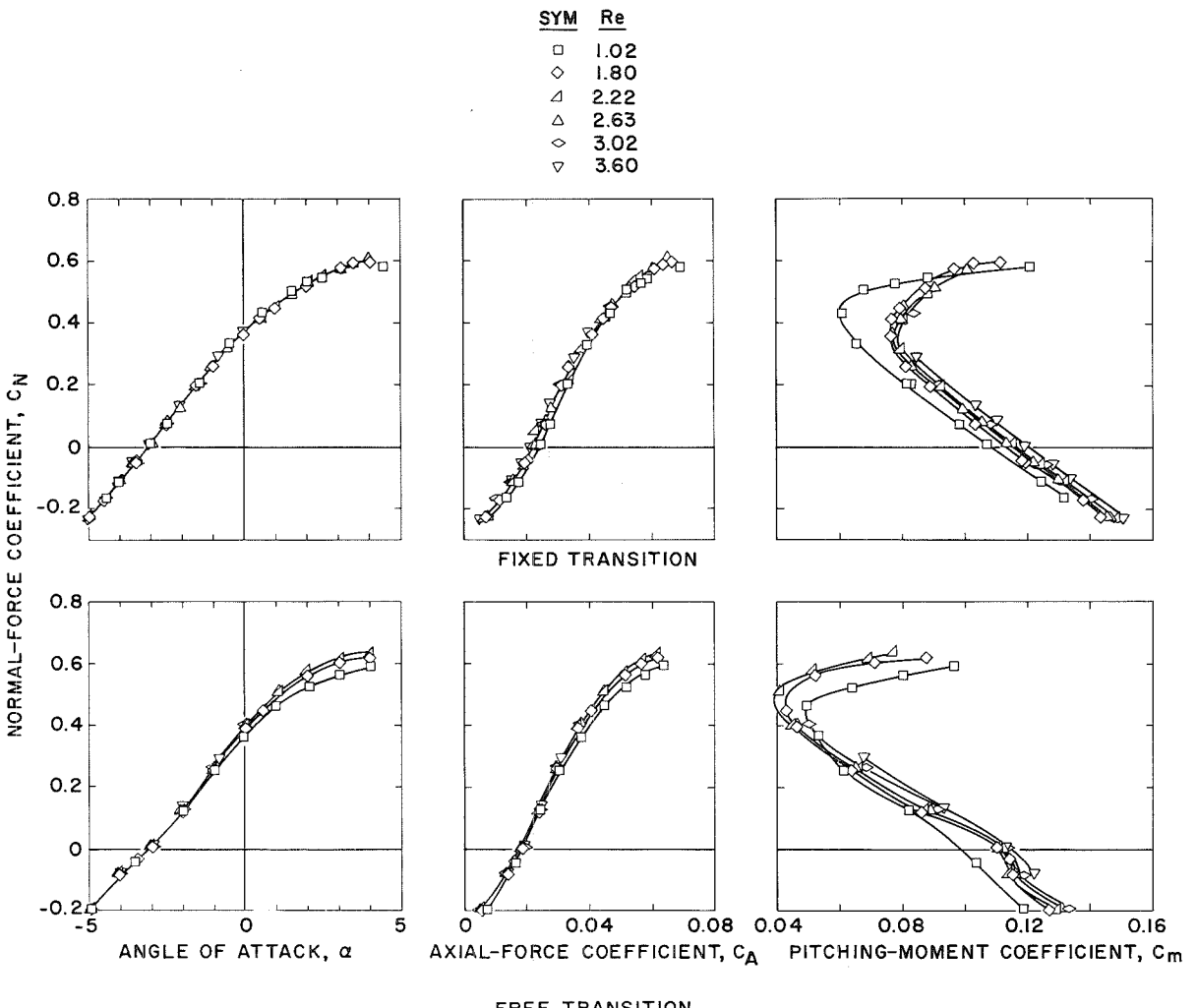

b. Tunnel 11TWT
Figure 7. Continued.

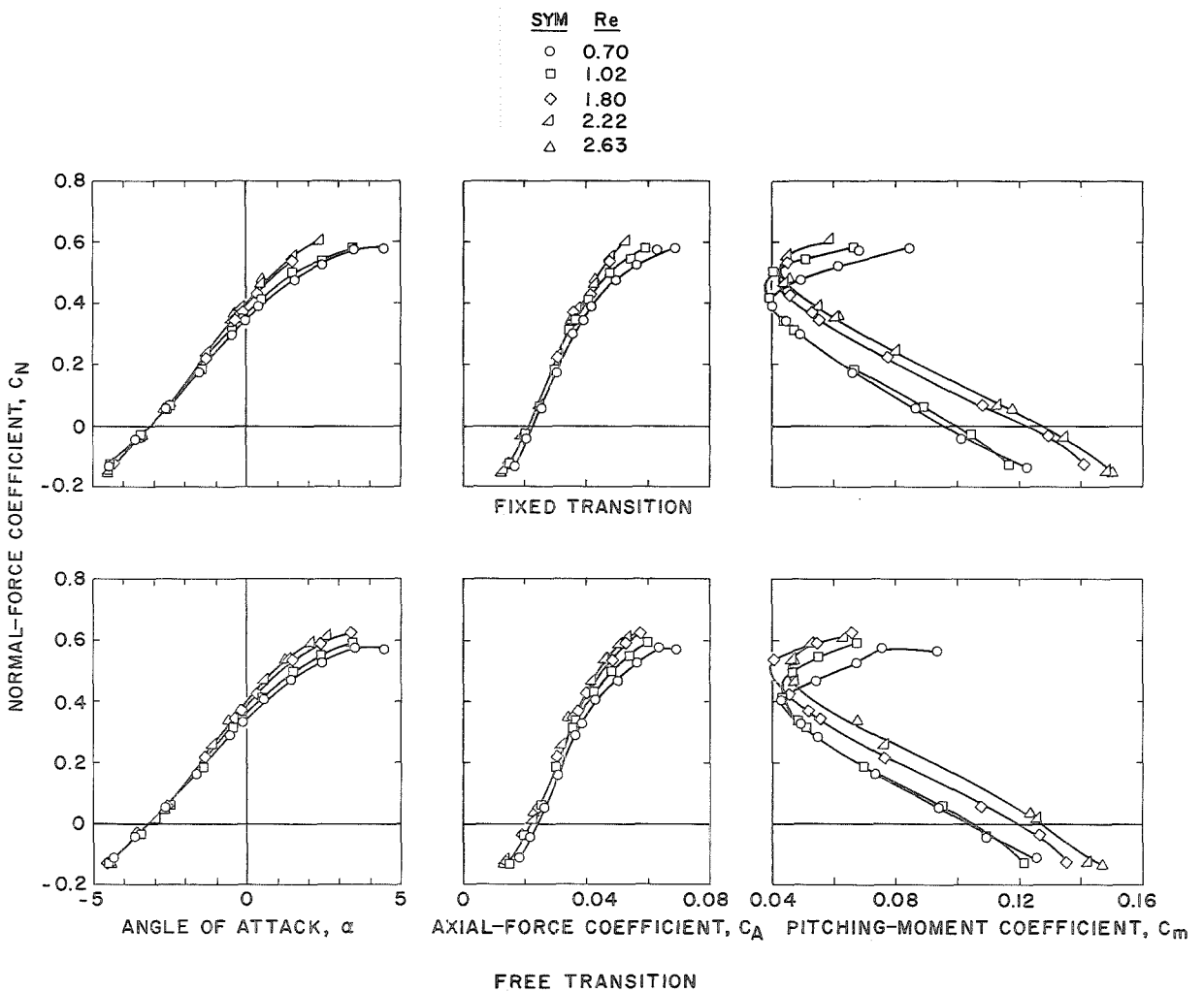

c. Tunnel 4T, τ = 5 percent
Figure 7. Concluded.

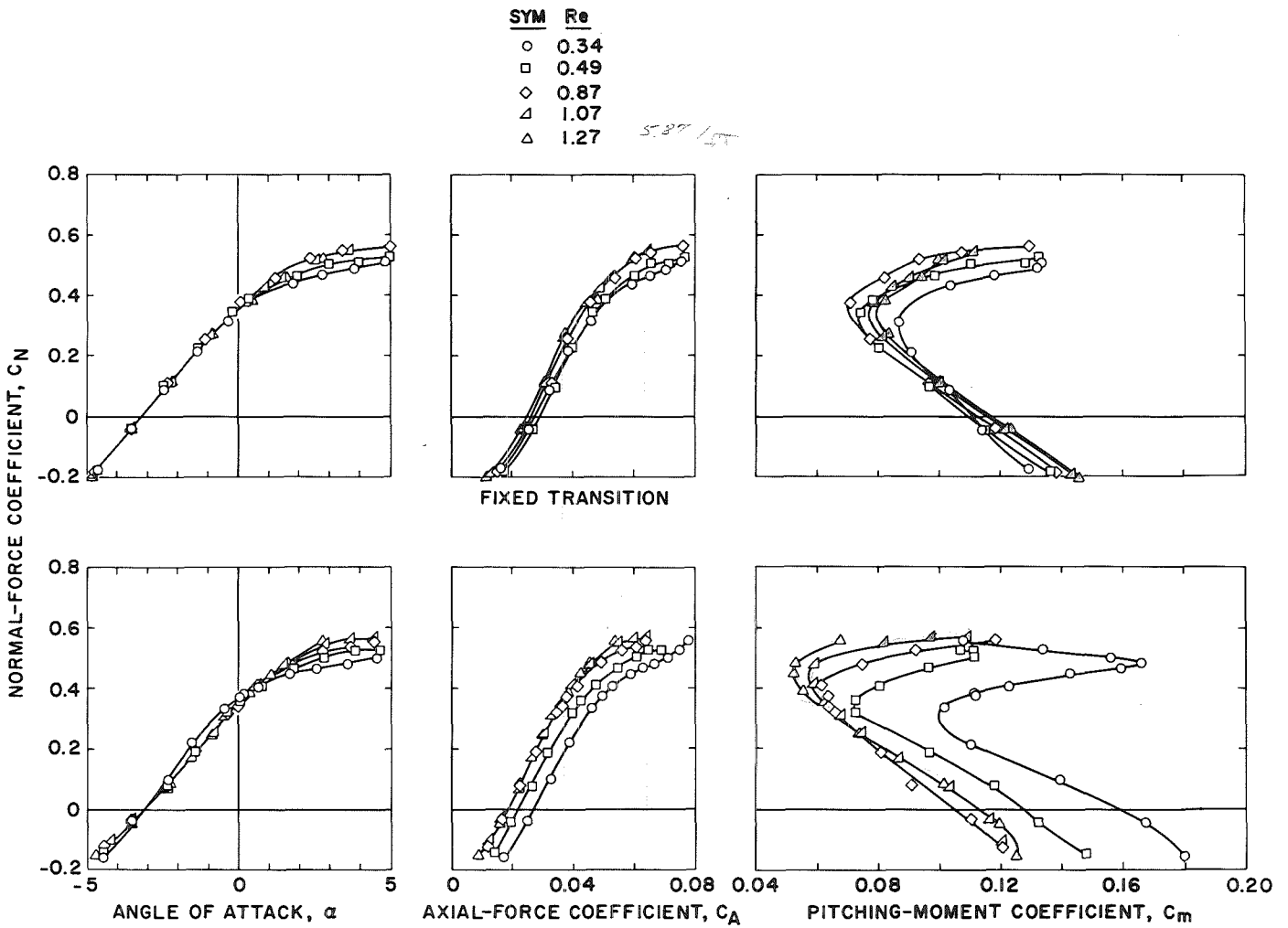

a. Tunnel 16T

Figure 8. Aerodynamic coefficients on the M3 model with fixed and free transition at $M_\infty = 0.84$ and various Reynolds numbers.

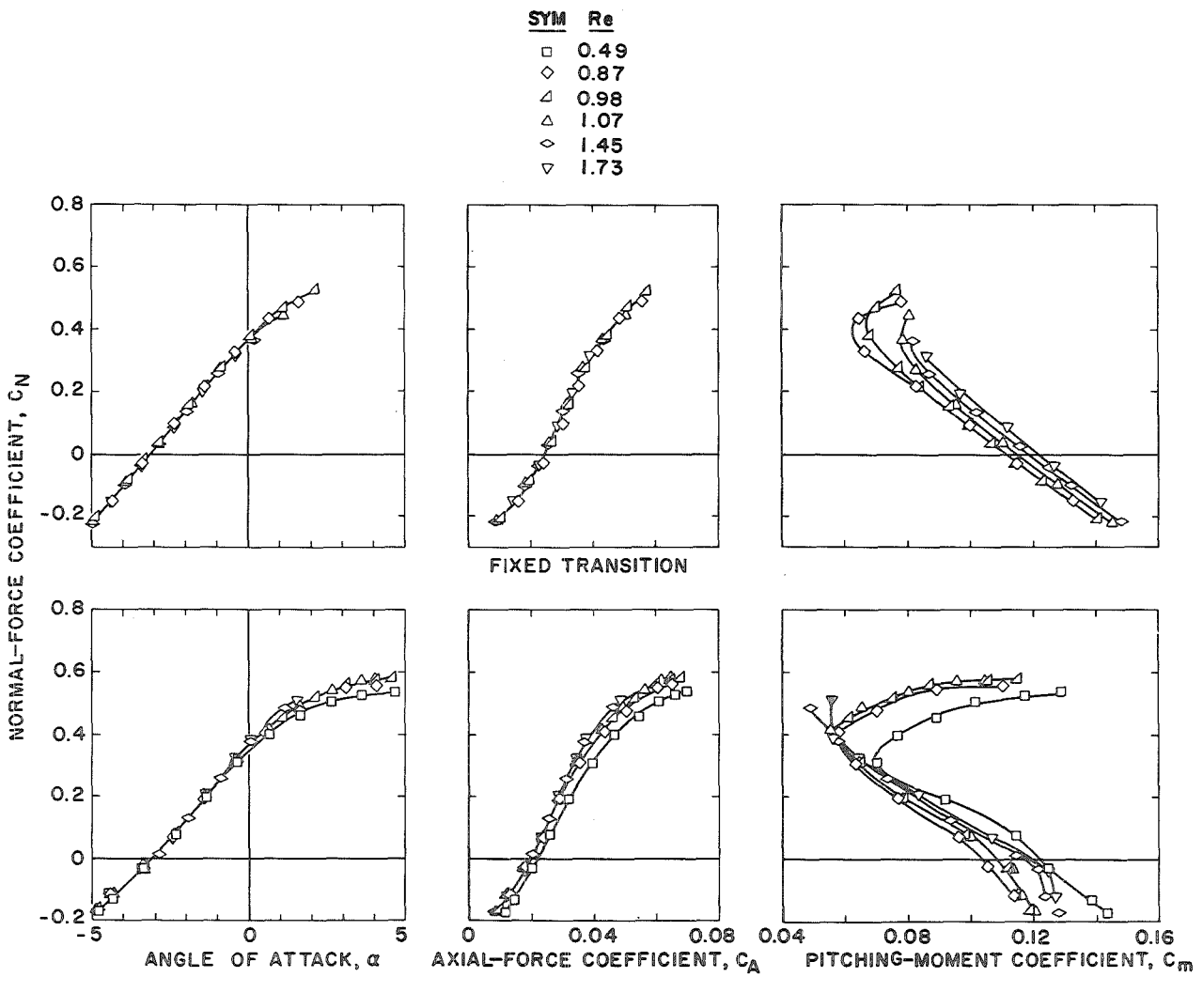

b. Tunnel 11TWT
Figure 8. Continued.

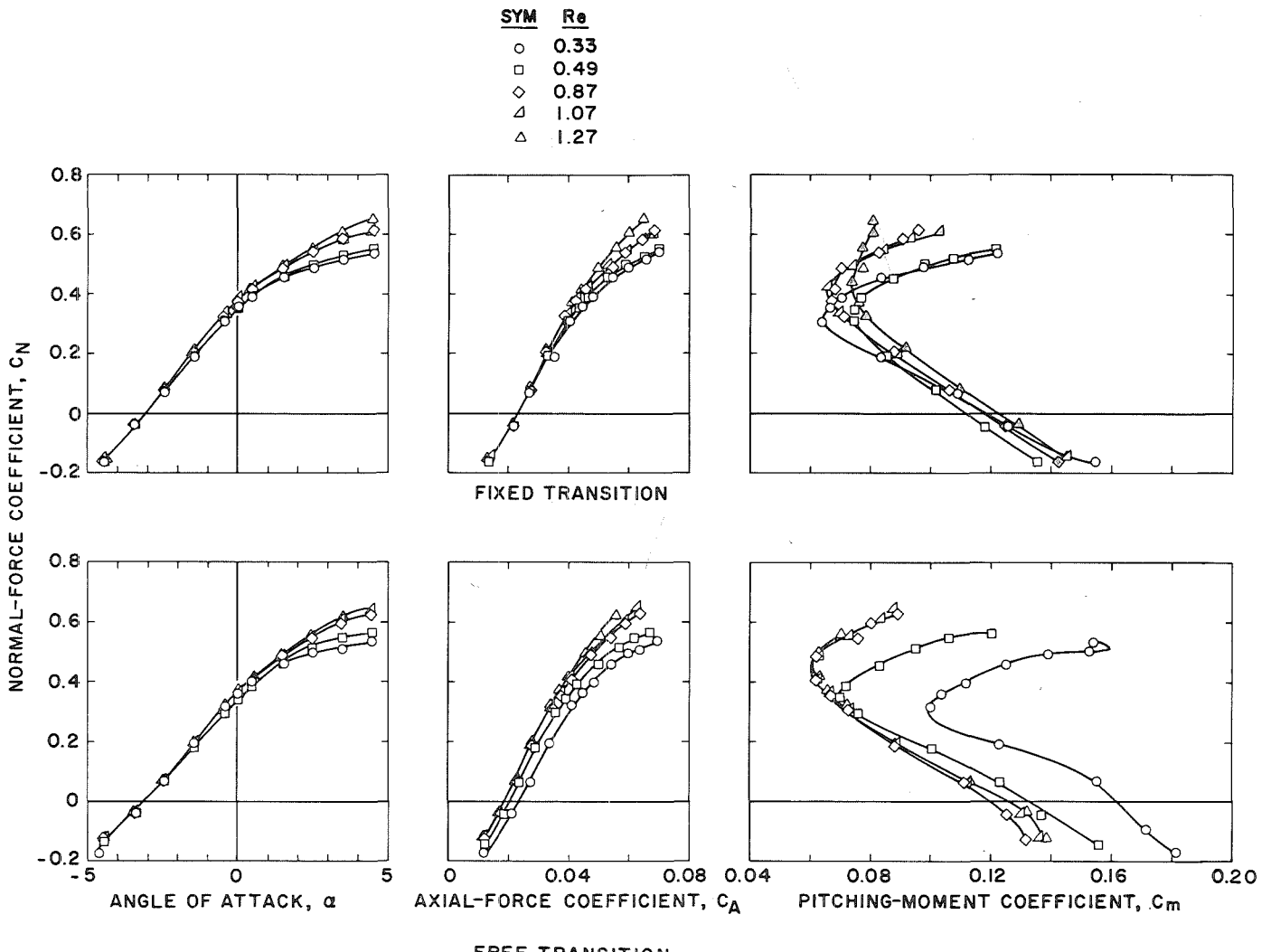

c. Tunnel 4T, τ = 5 percent
Figure 8. Concluded.

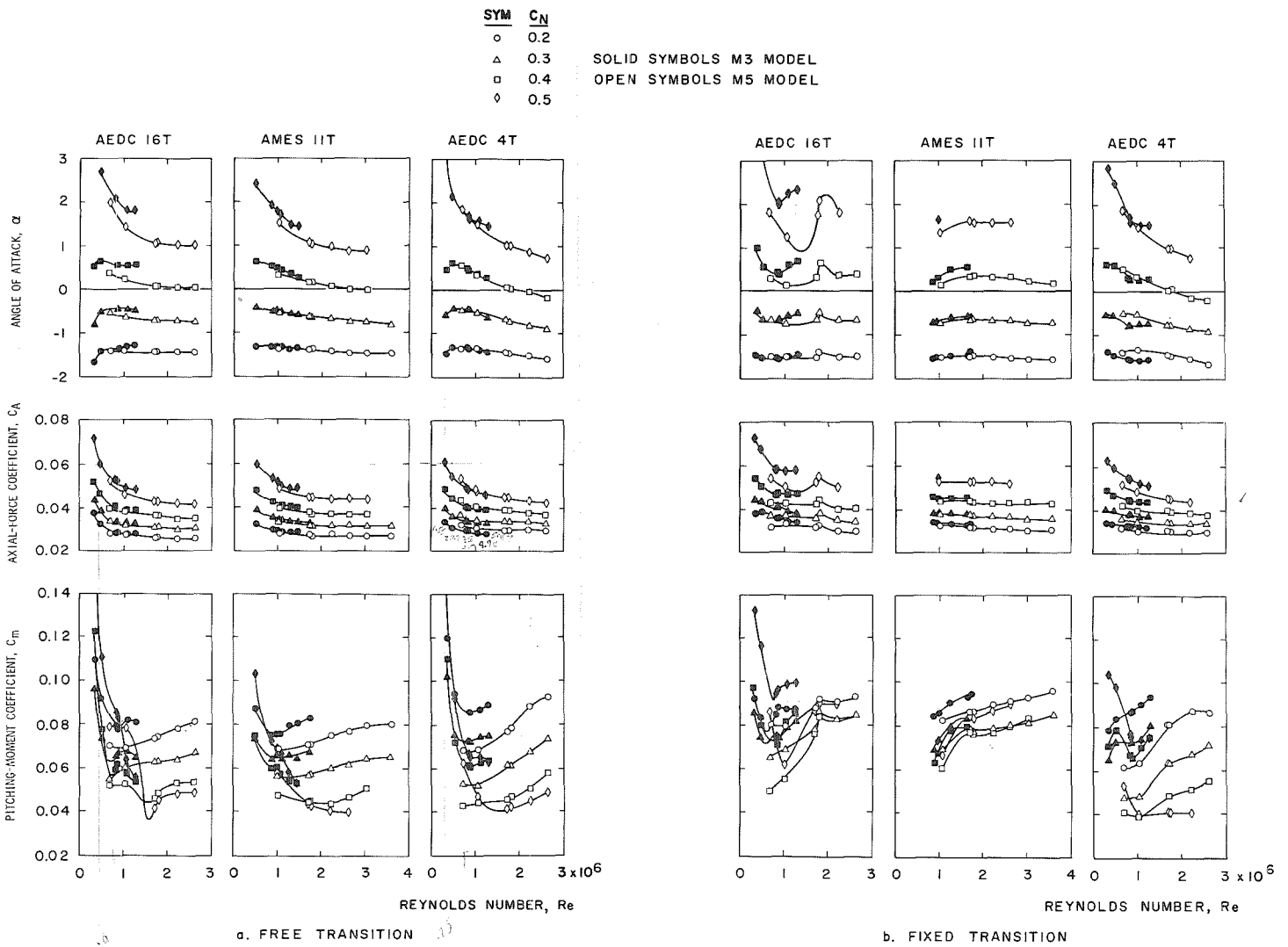

a. Free transition

b. Fixed transition

Figure 9. Effect of Reynolds number on the ONERA model data in the three wind tunnels.

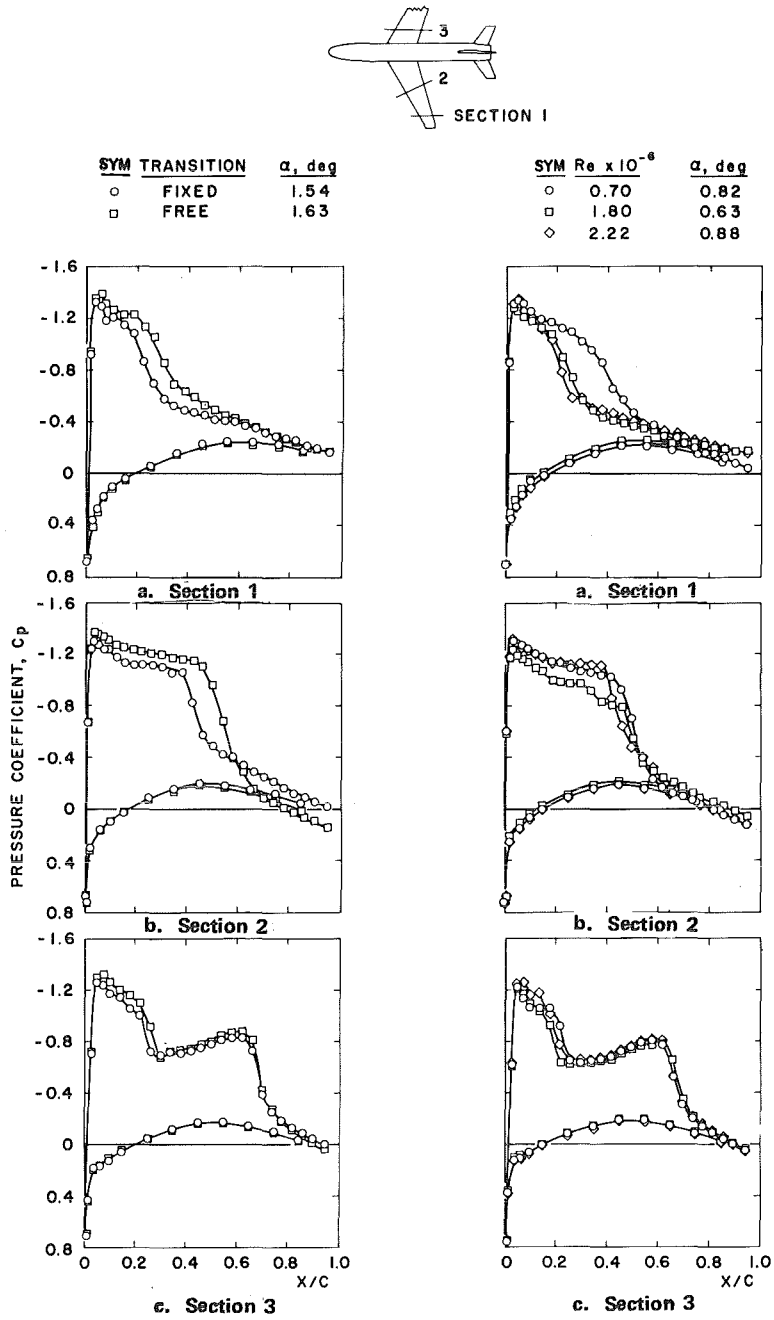

Figure 10. Effect of fixing transition on the M5 wing pressure distribution in Tunnel 16T, $M_\infty = 0.84$, $Re = 1.80 \times 10^6$.

Figure 11. Effect of Reynolds number on the M5 wing pressure distribution with fixed transition in Tunnel 16T, $M_\infty = 0.84$.

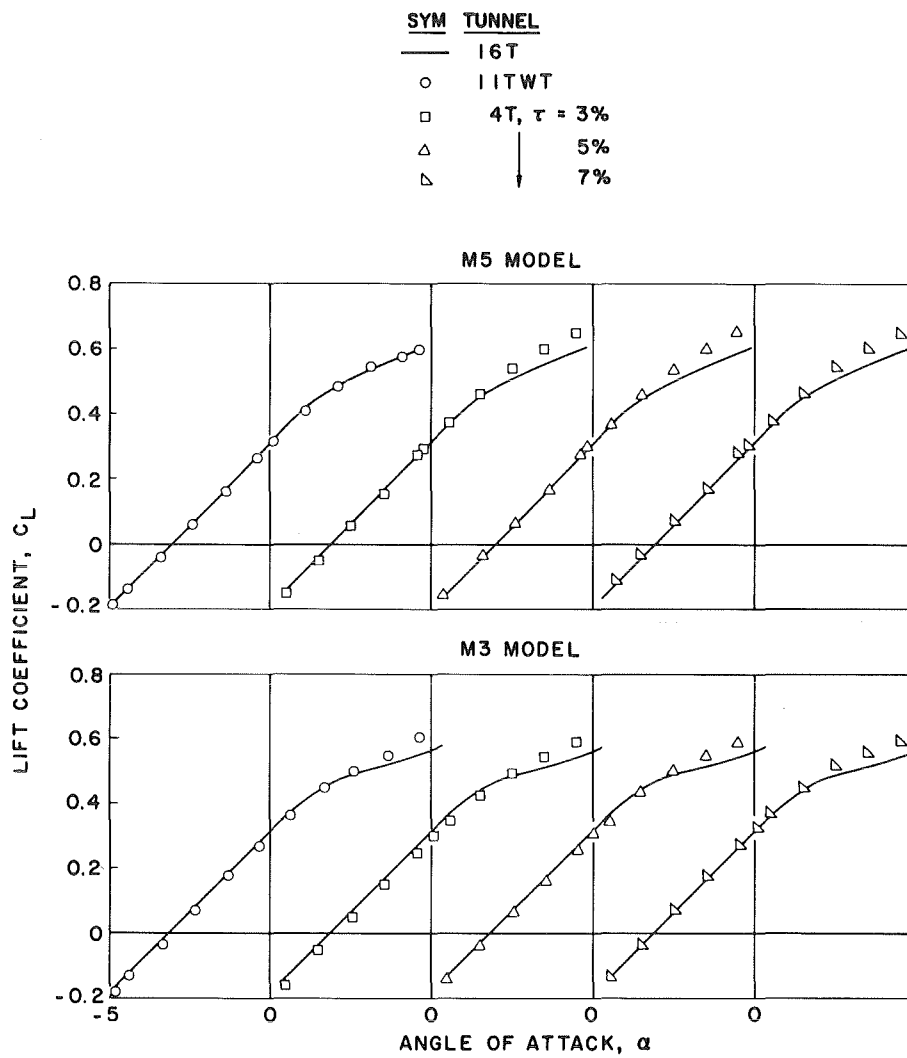

a. Lift coefficient

Figure 12. Comparison of force and moment coefficients at $M_\infty = 0.7$ in Tunnels 16T, 11TWT, and 4T.

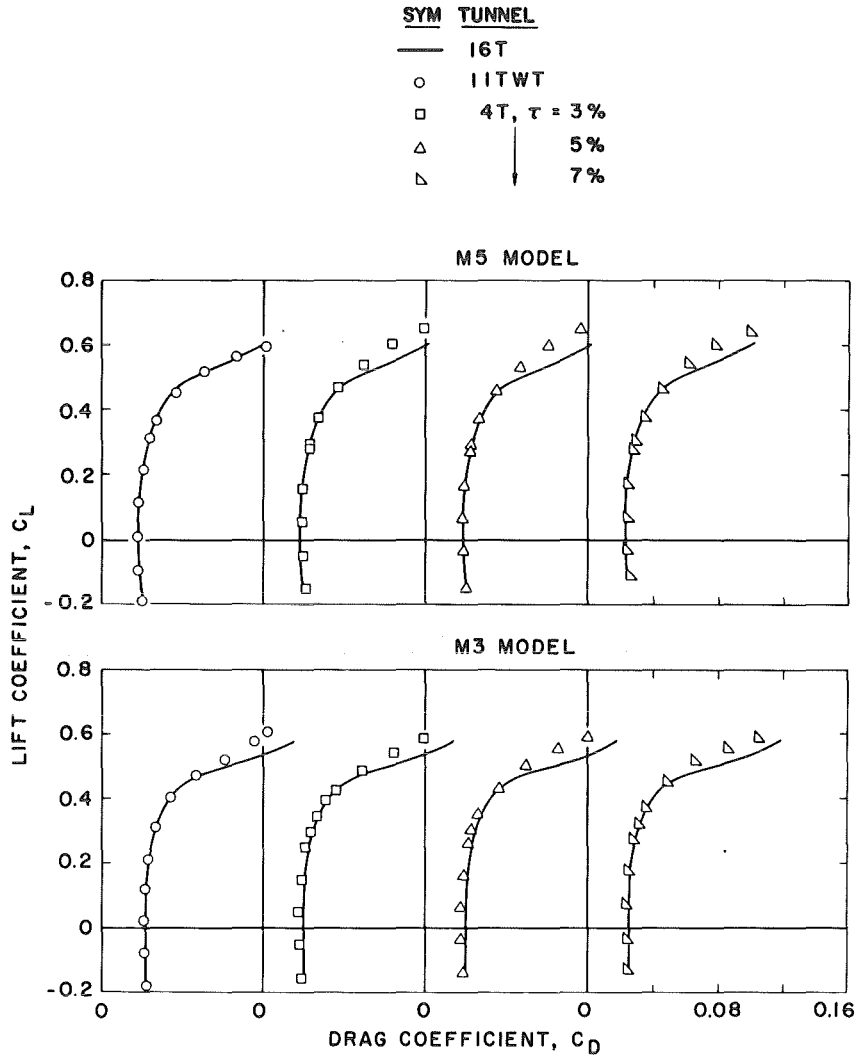

b. Drag coefficient
Figure 12. Continued.

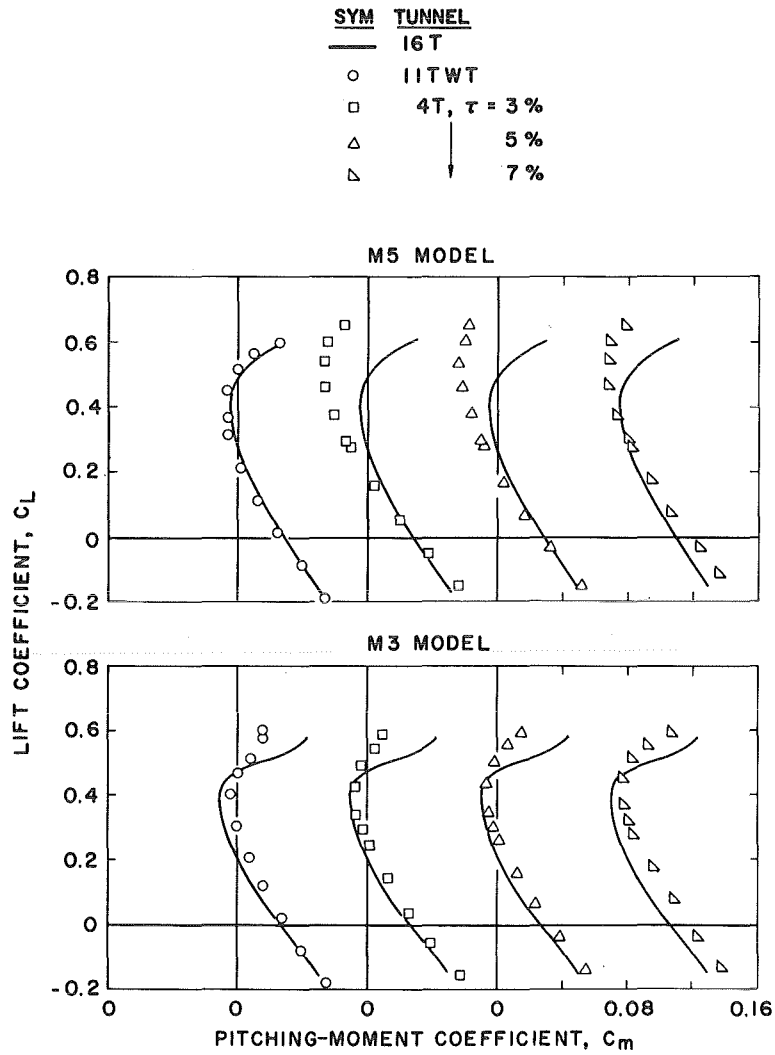

c. Pitching-moment coefficient
Figure 12. Concluded.

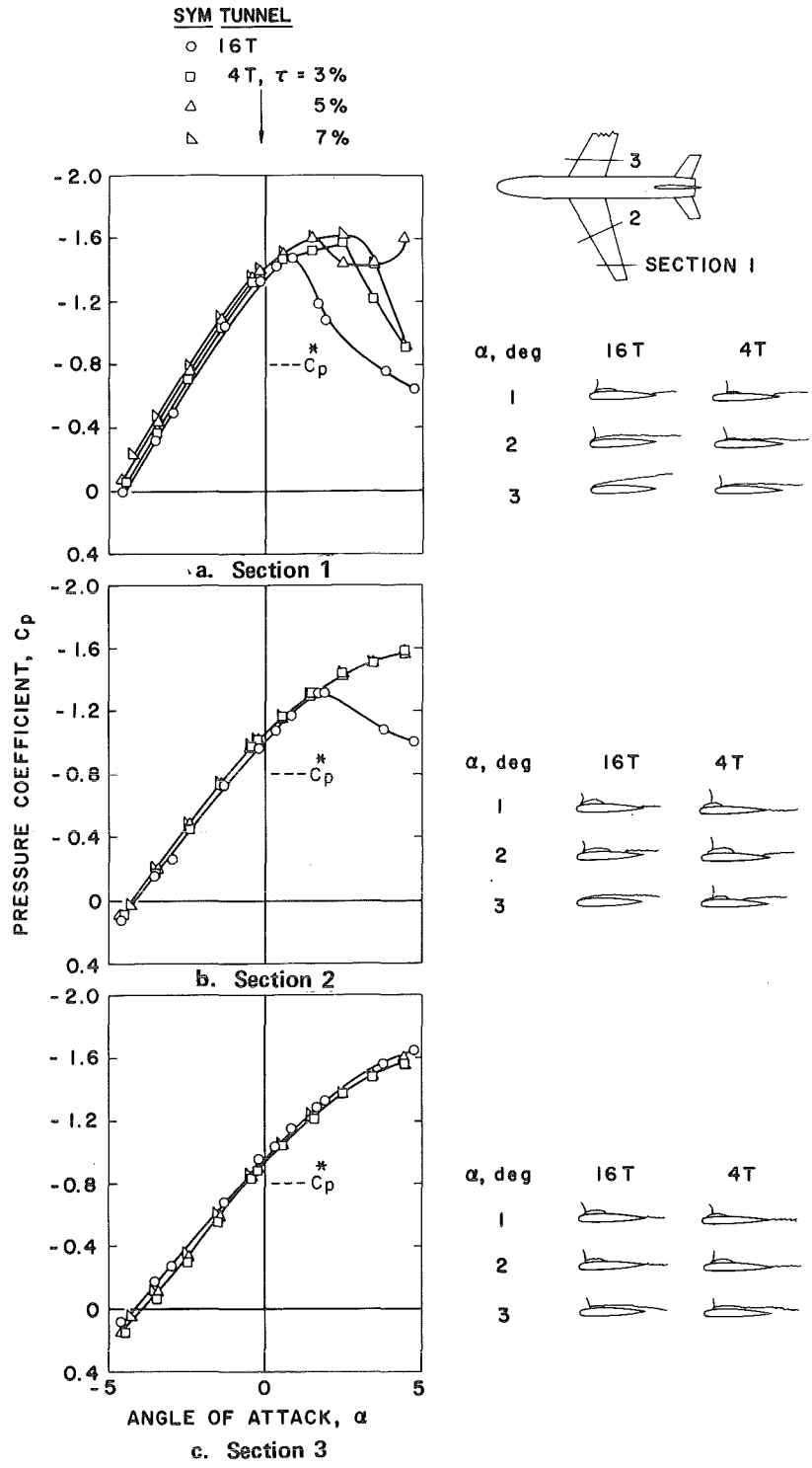

Figure 13. Pressure at x/c = 0.01 and separation pattern on the M5 wing at M_∞ = 0.7 in Tunnels 16T and 4T.

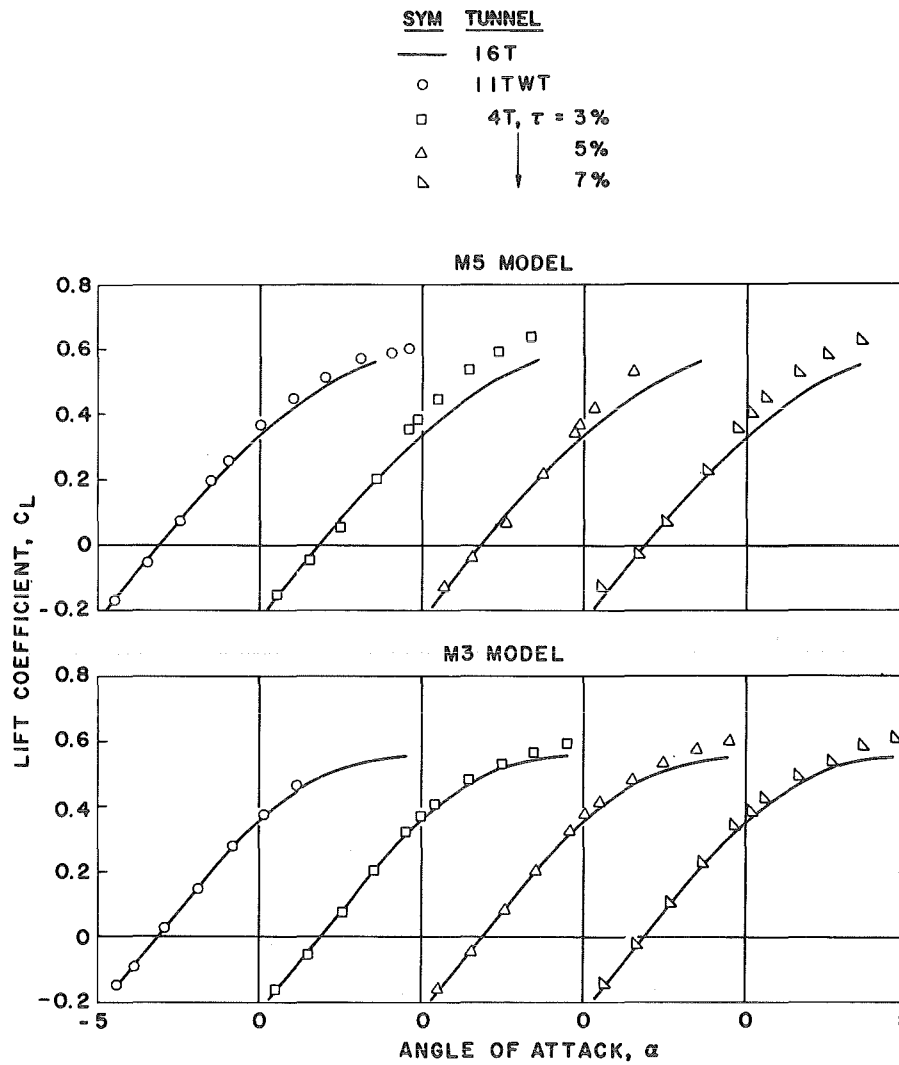

a. Lift coefficient

Figure 14. Force and moment coefficients at $M_\infty = 0.84$ in Tunnels 16T, 11TWT, and 4T.

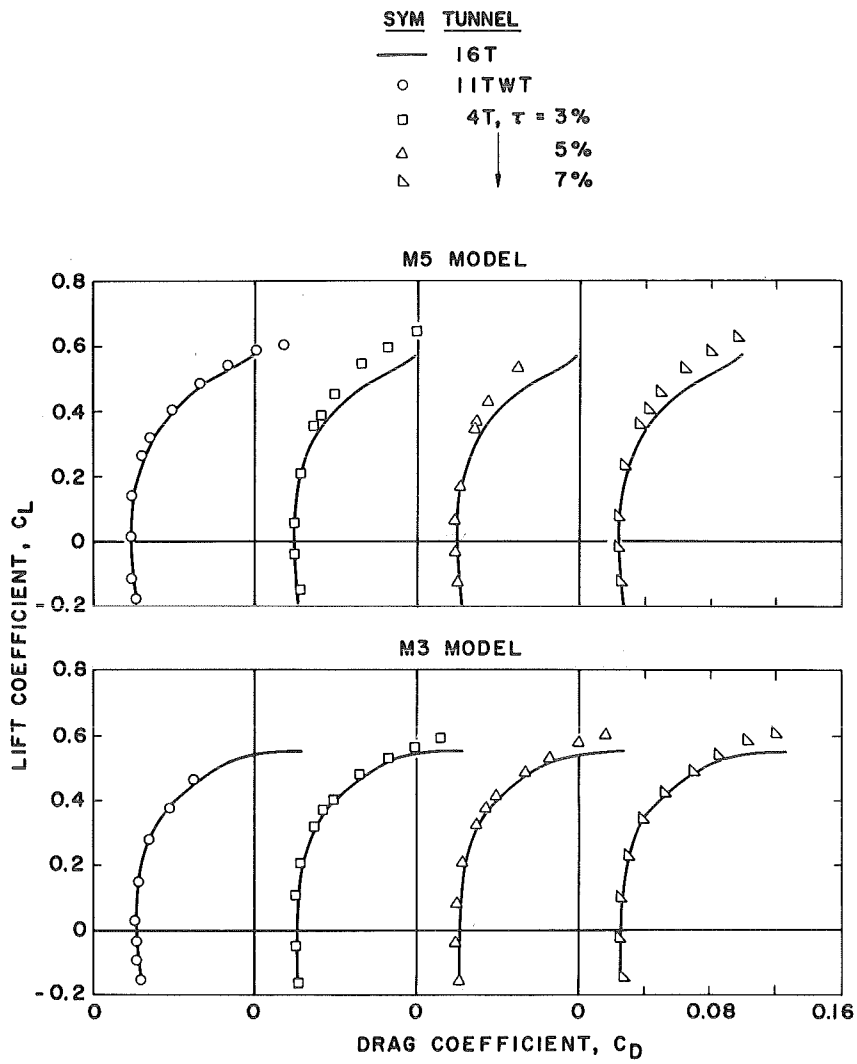

b. Drag coefficient
Figure 14. Continued.

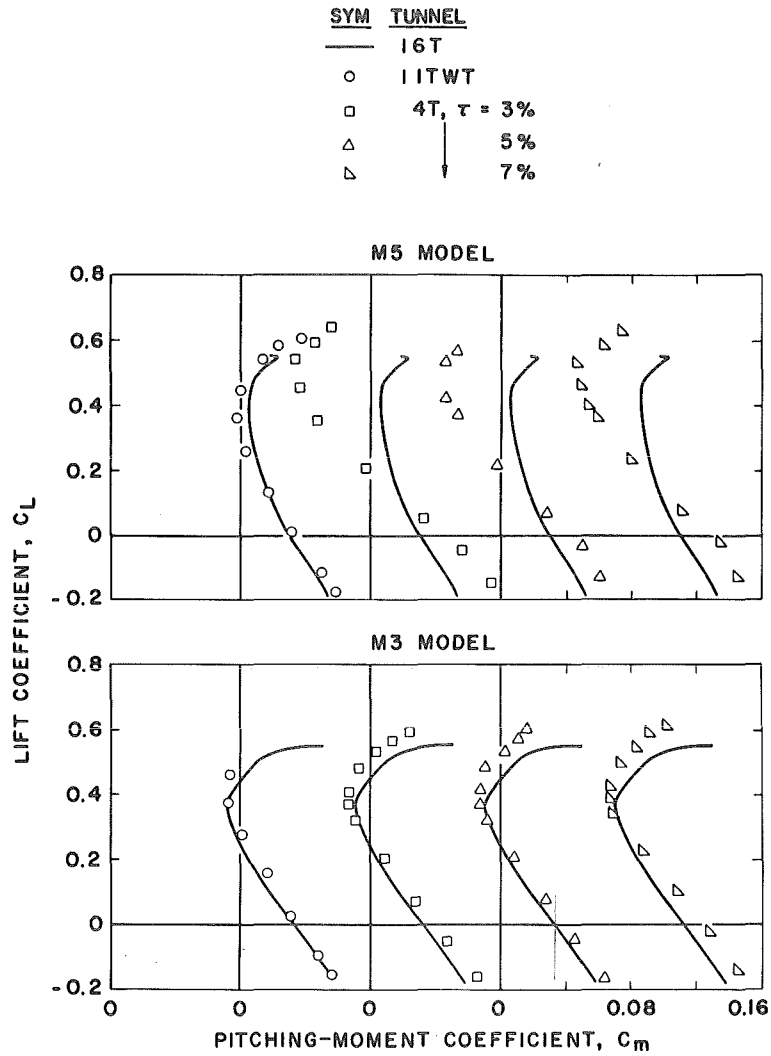

c. Pitching–moment coefficient
Figure 14. Concluded.

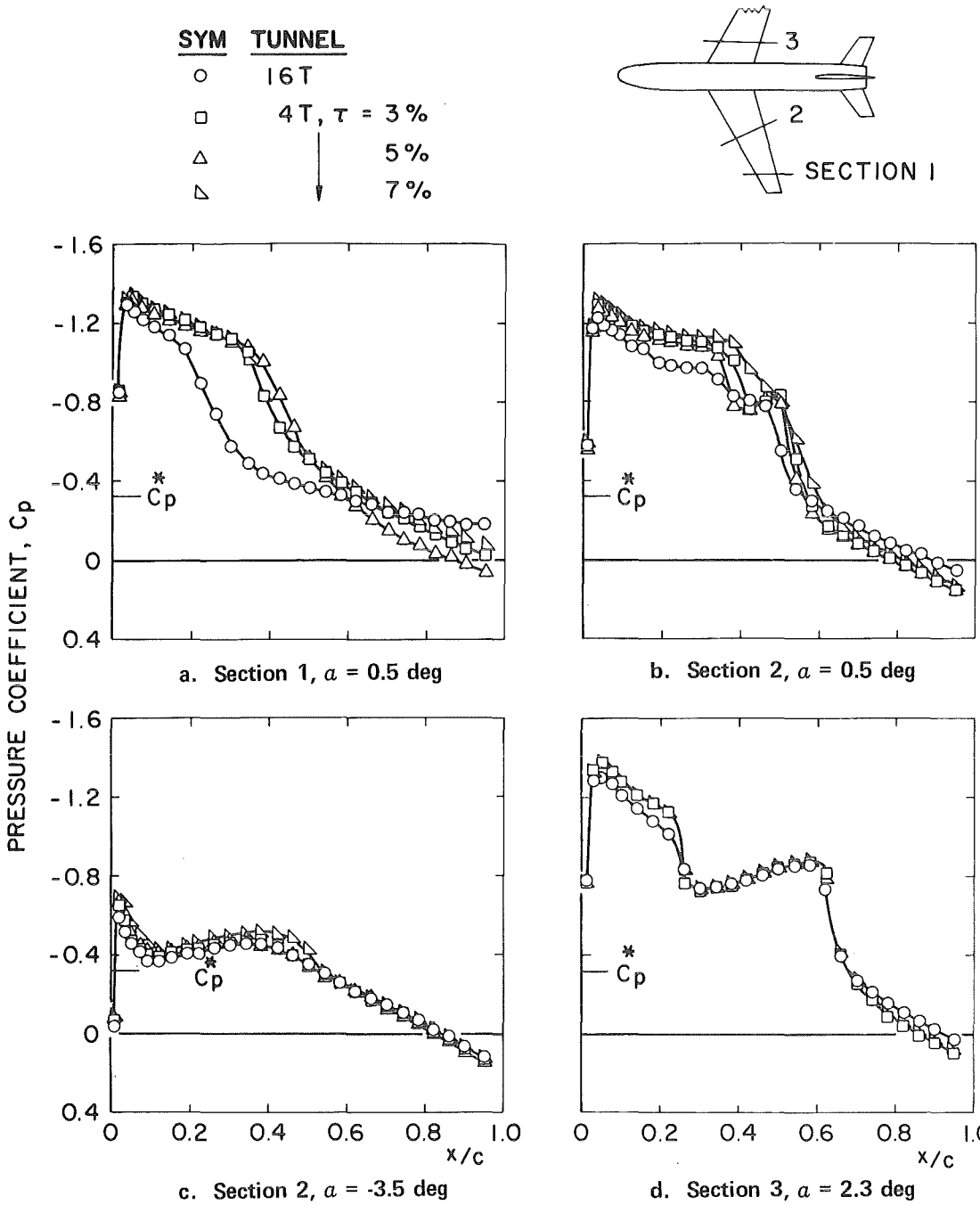

a. Section 1, α = 0.5 deg

b. Section 2, α = 0.5 deg

c. Section 2, α = -3.5 deg

d. Section 3, α = 2.3 deg

Figure 15. Selected M5 wing pressure distributions at M_∞ = 0.84.

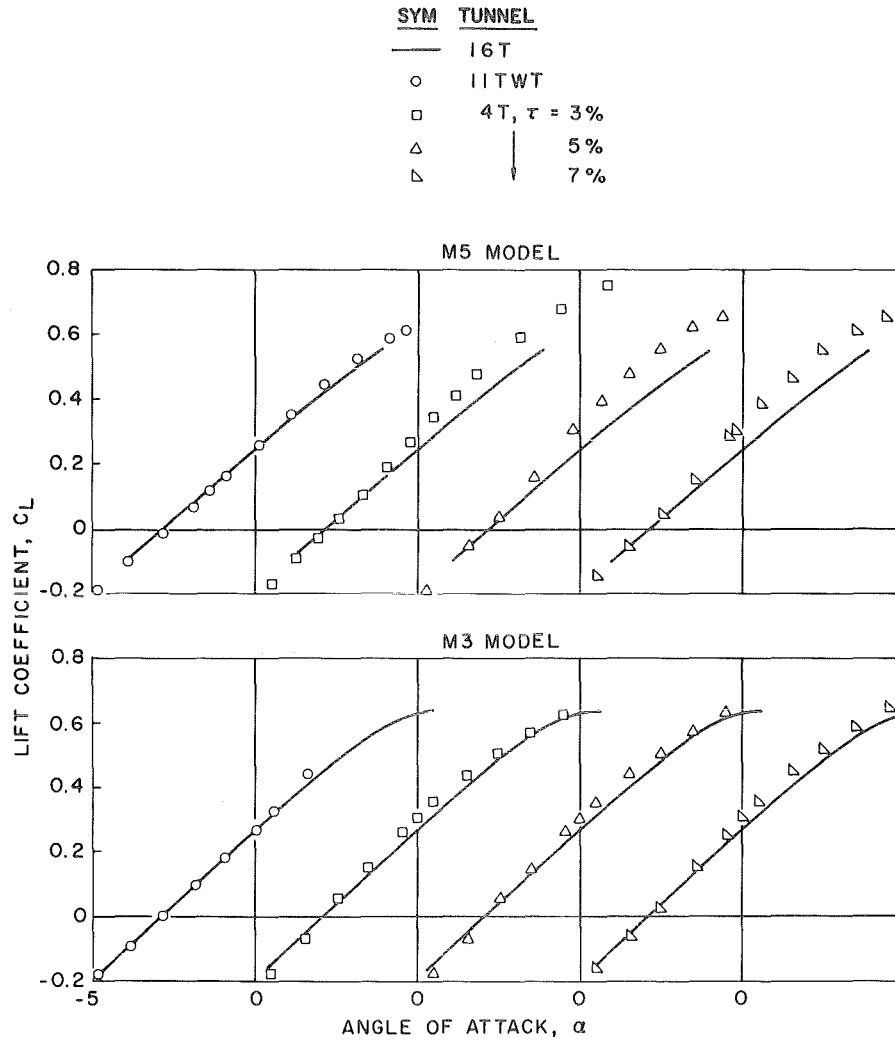

a. Lift coefficient

Figure 16. Force and moment coefficients at M_∞ = 0.90 in Tunnels 16T, 11TWT, and 4T.

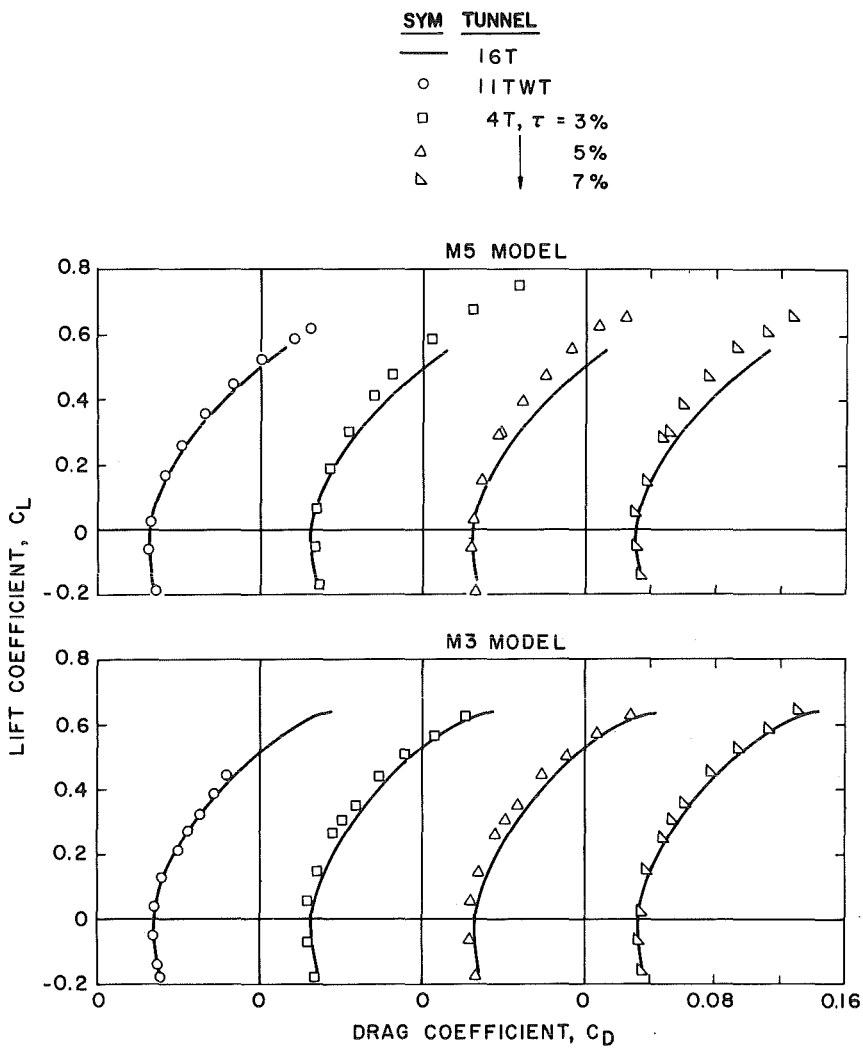

b. Drag coefficient
Figure 16. Continued.

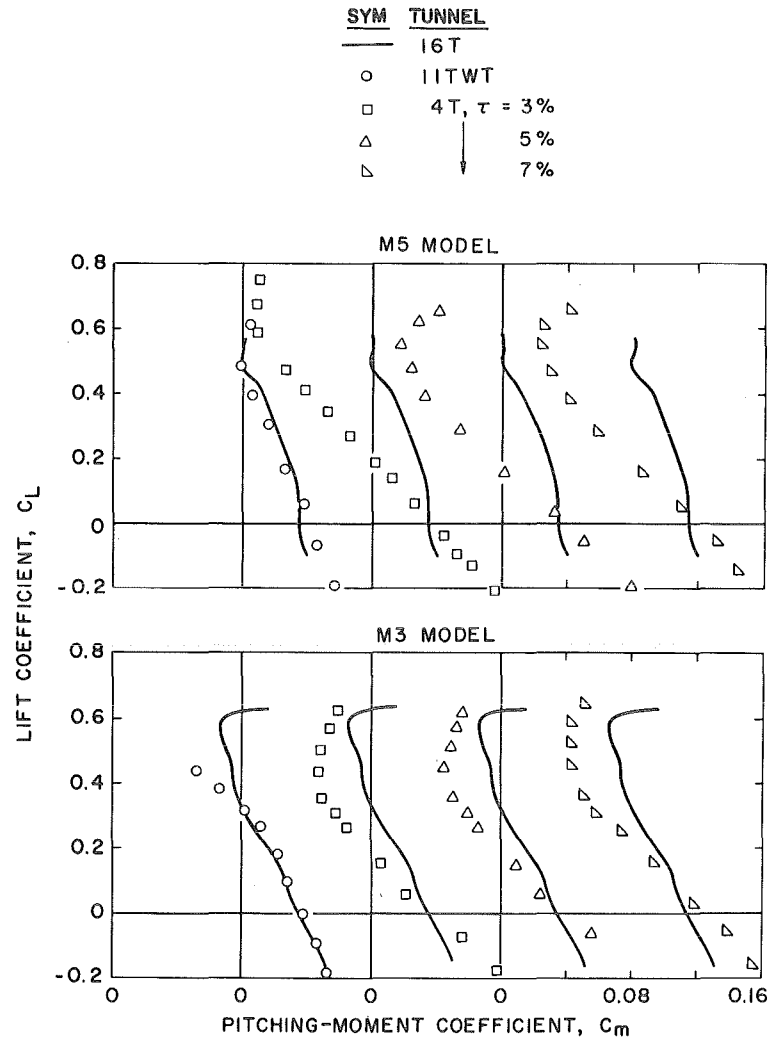

c. Pitching—moment coefficient
Figure 16. Concluded.

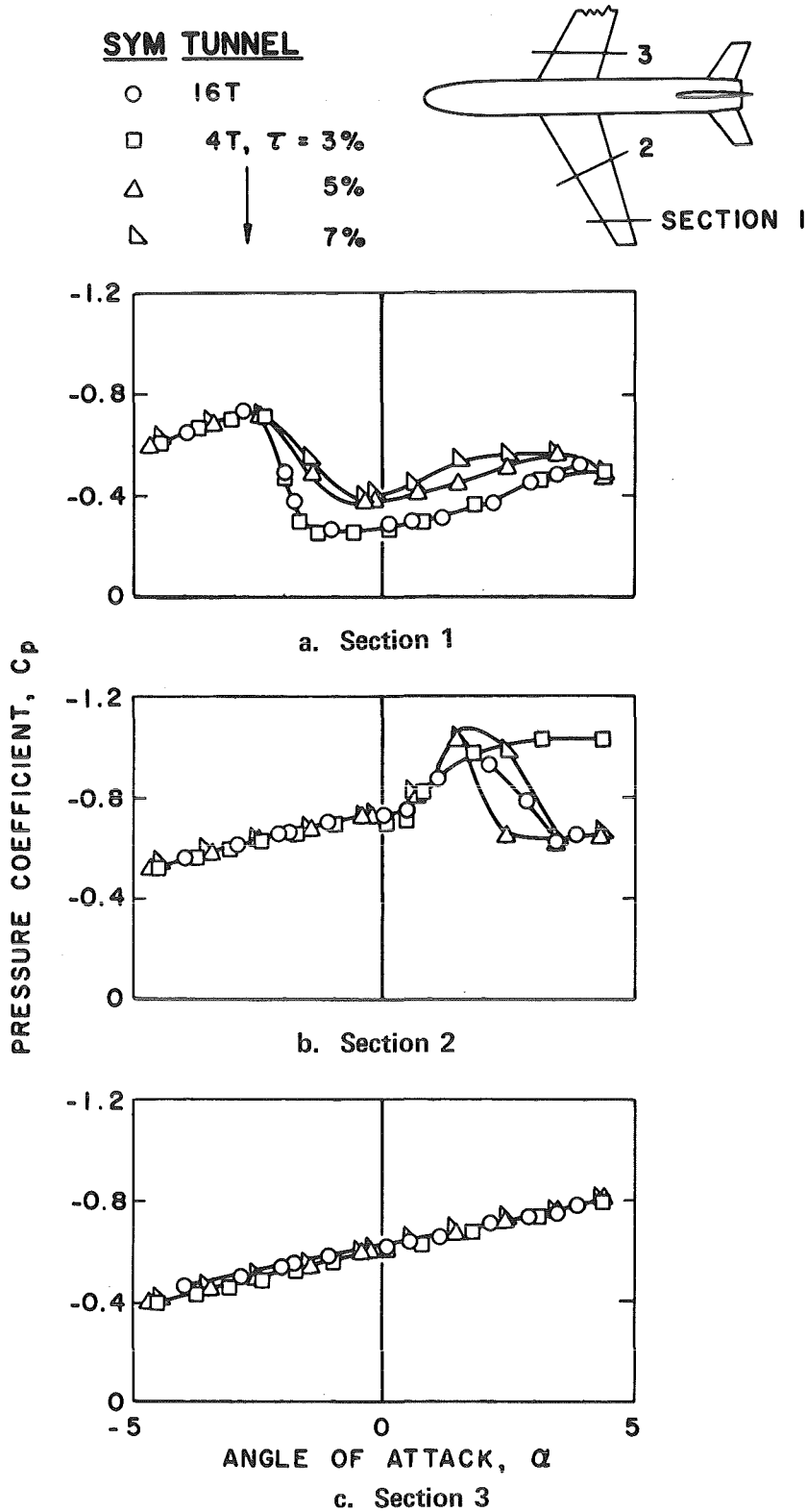

Figure 17. M5 wing pressure coefficients at x/c = 0.46 in Tunnels 16T and 4T, M_∞ = 0.90.

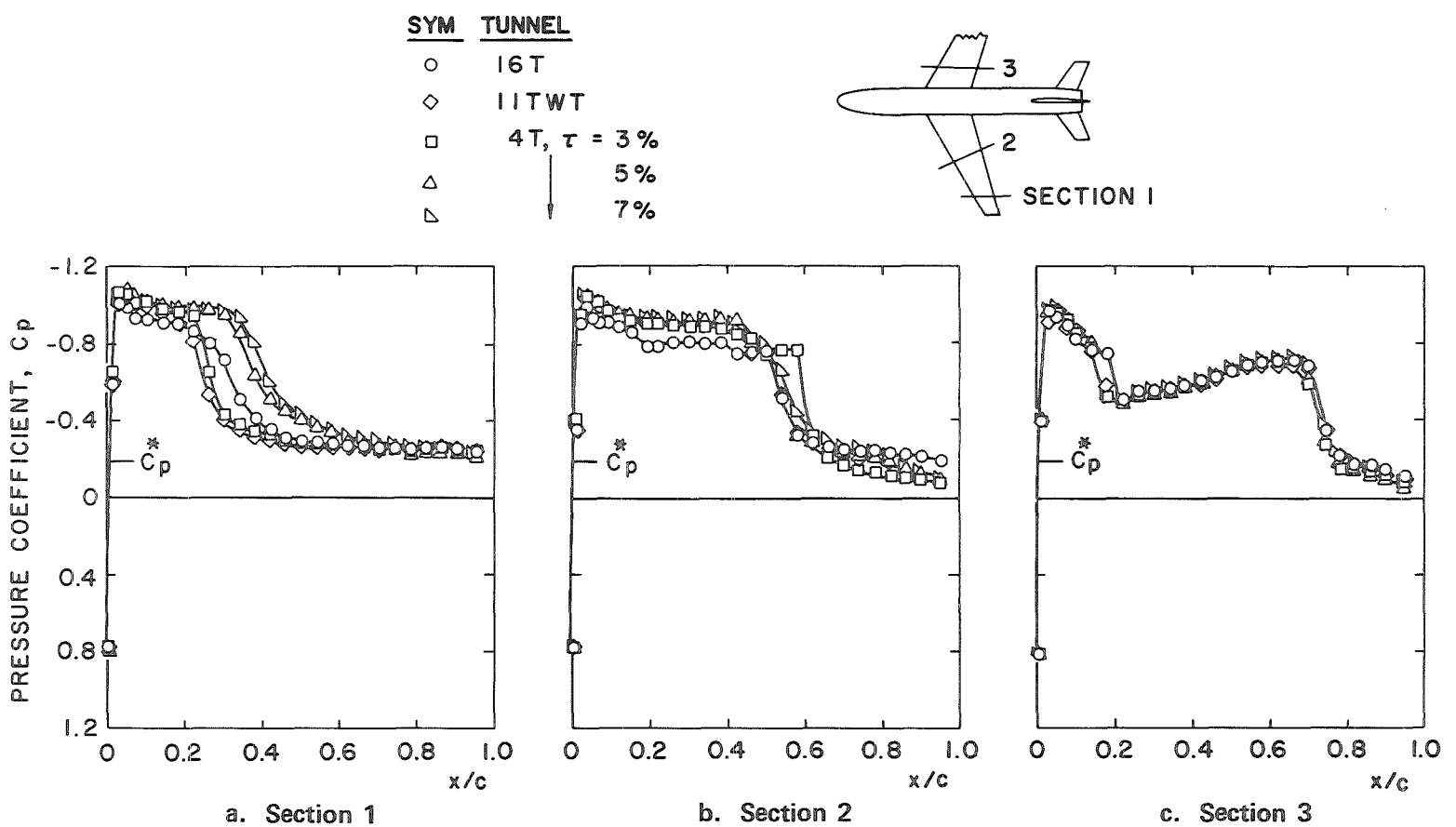

Figure 18. Representative M5 wing pressure distribution at $M_\infty = 0.9$, $\alpha = 0.5$ deg.

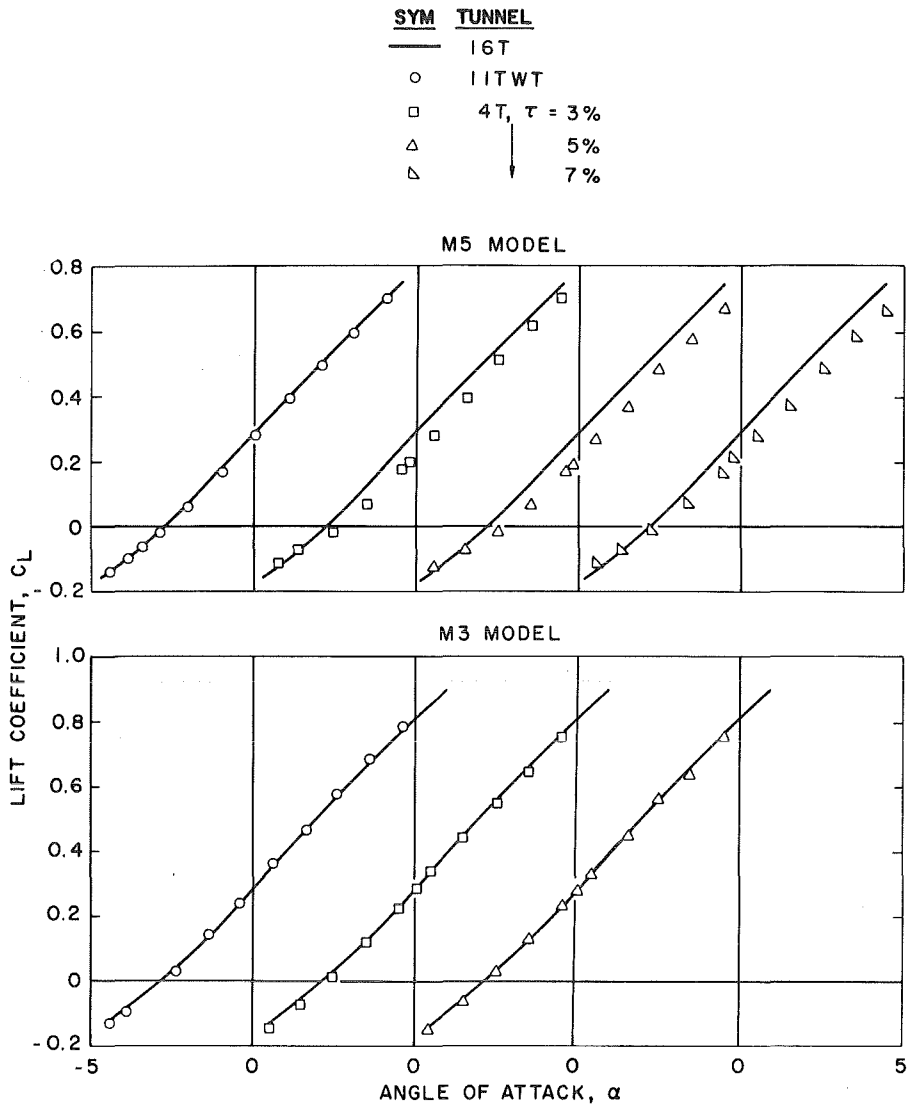

a. Lift coefficient

Figure 19. Force and moment coefficients at M_∞ = 0.95 in Tunnels 16T, 11TWT, and 4T.

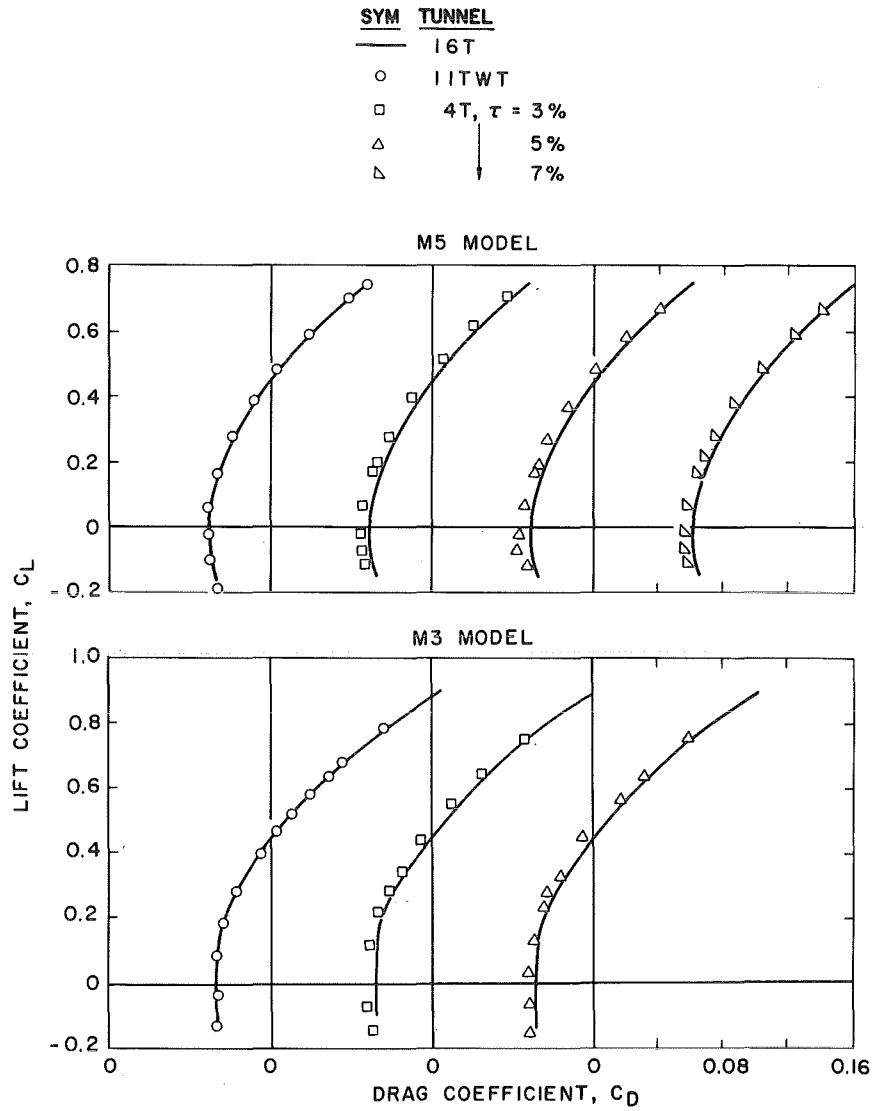

b. Drag coefficient
Figure 19. Continued.

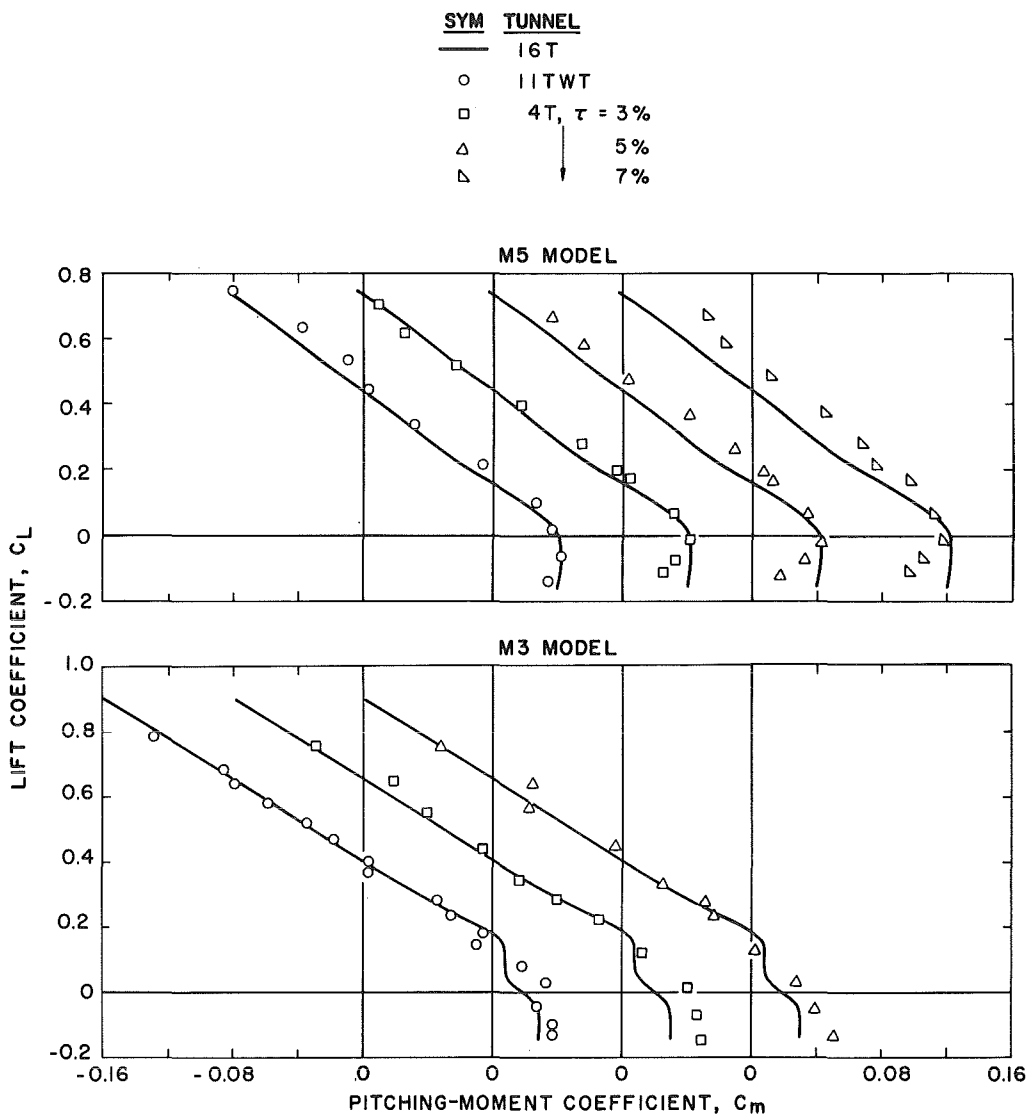

c. Pitching—moment coefficient
Figure 19. Concluded.

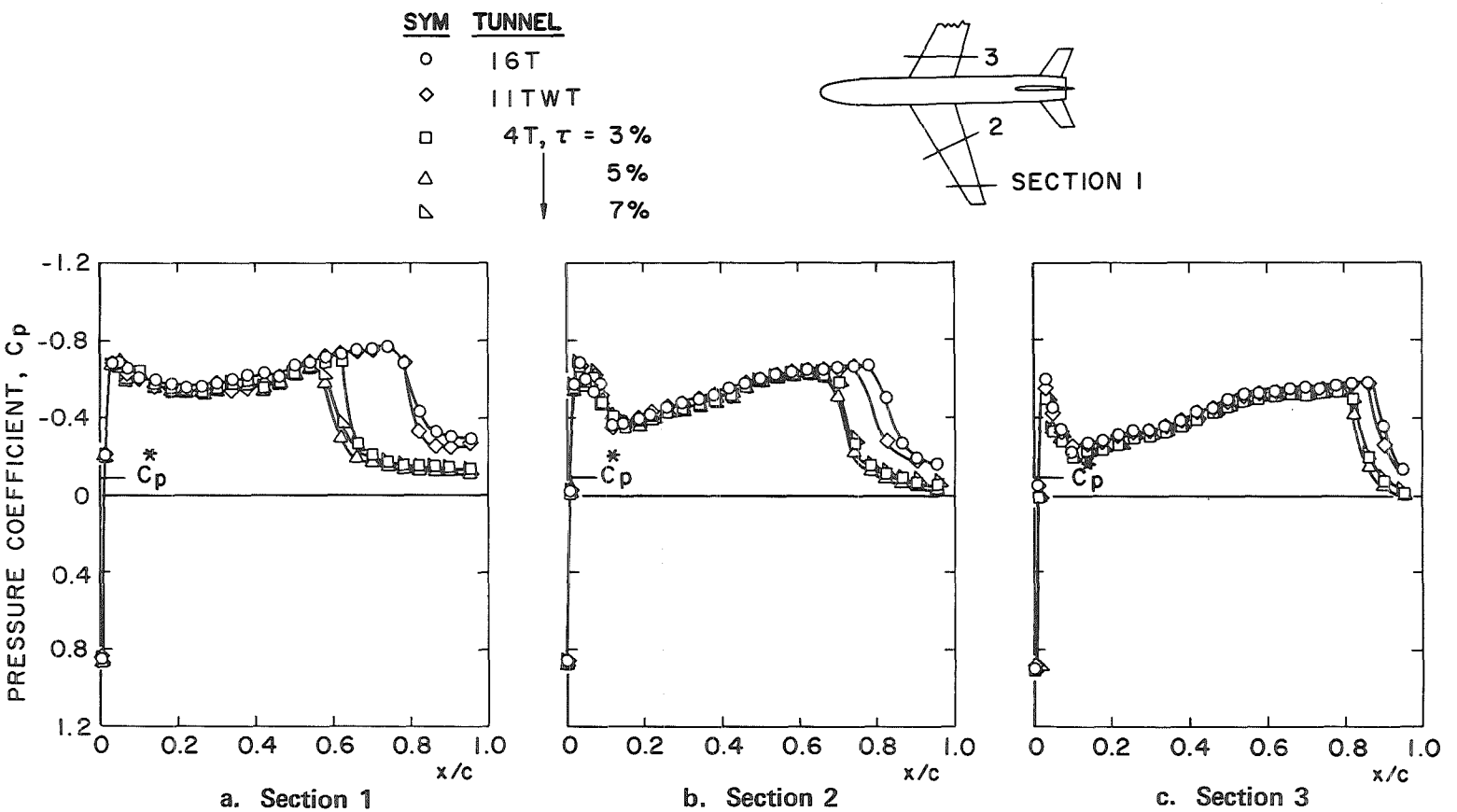

Figure 20. M5 wing pressure distribution at M_∞ = 0.95, zero lift.

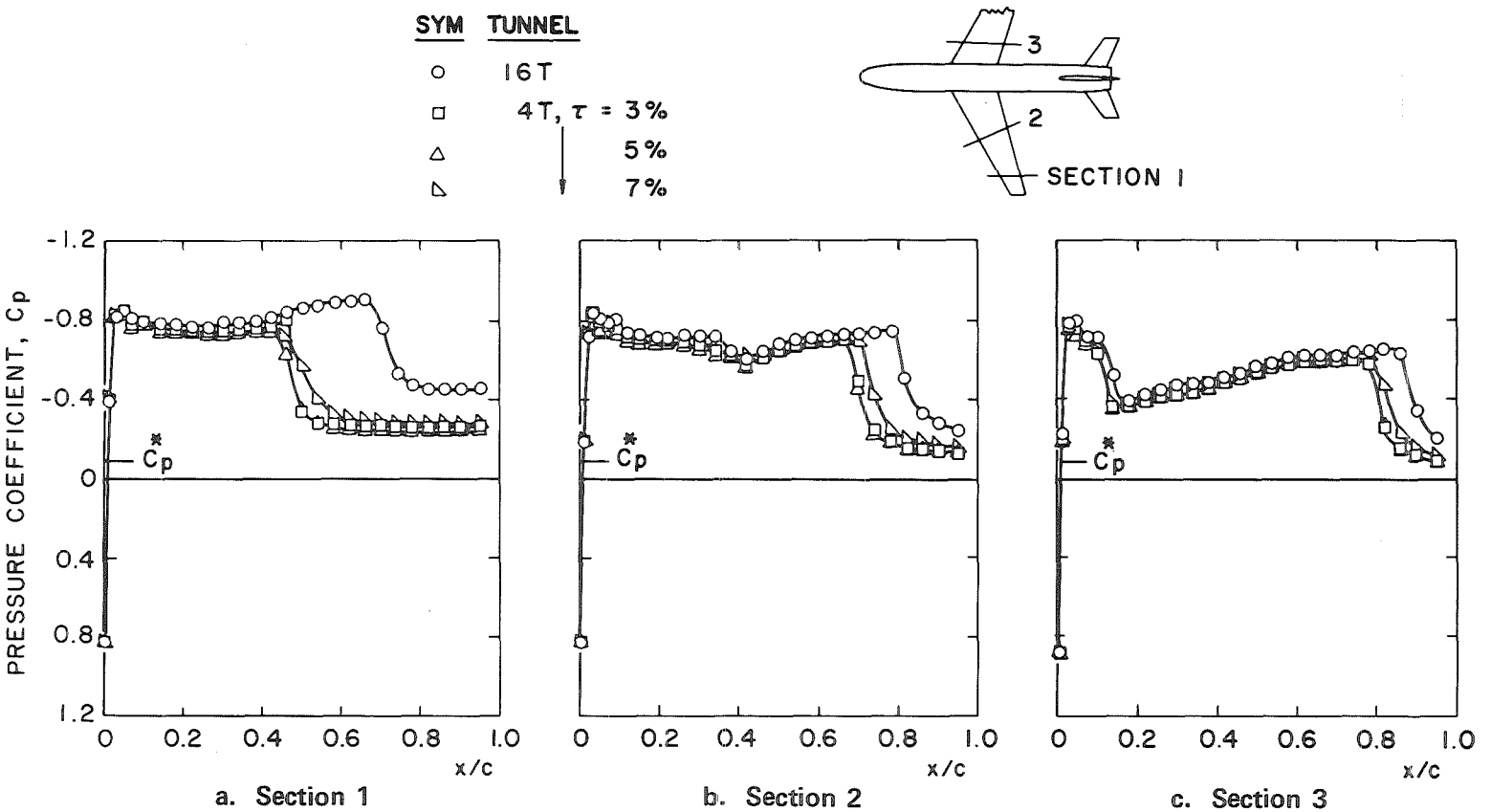

Figure 21. Representative M5 wing pressure distribution at M_∞ = 0.95, α = -2 deg.

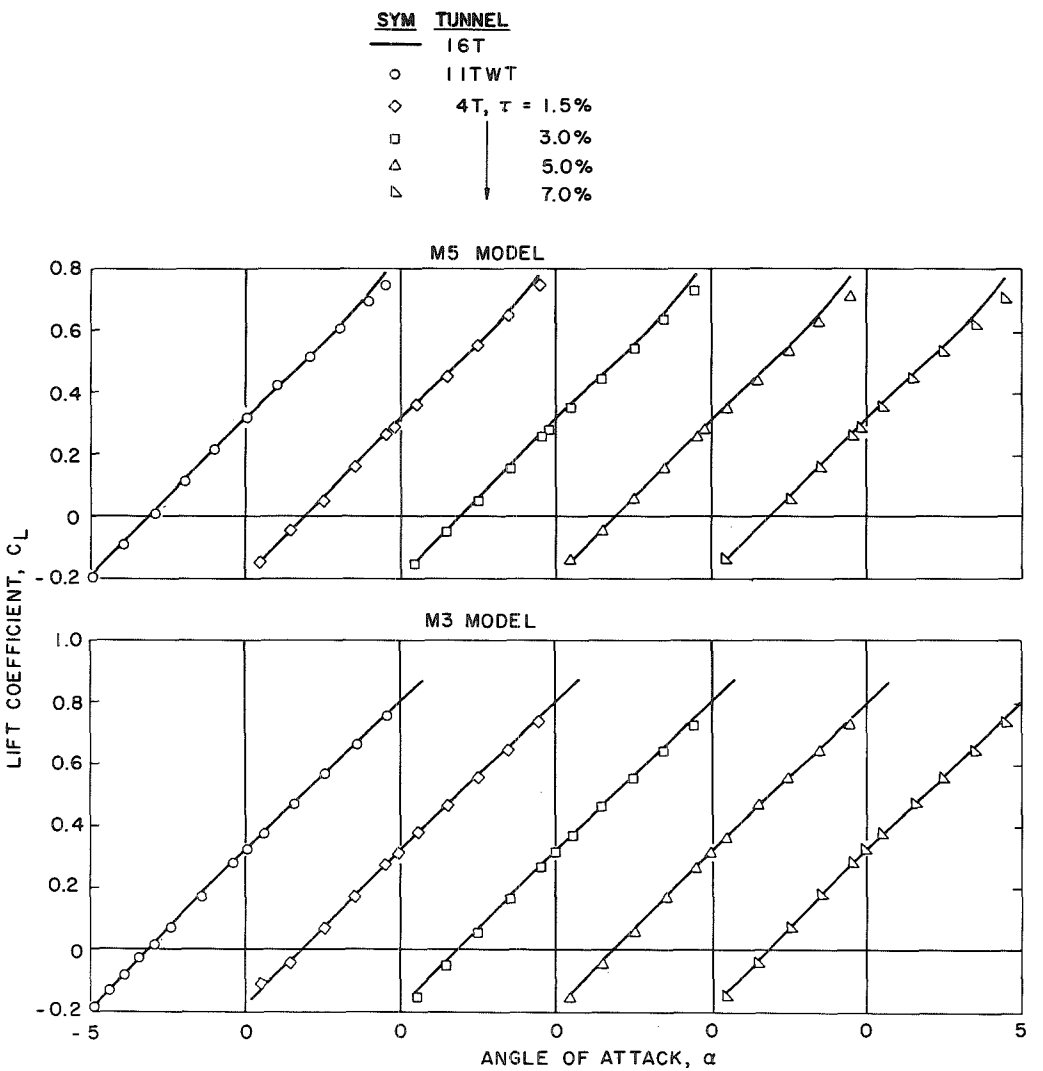

a. Lift coefficient

Figure 22. Force and moment coefficients at M_∞ = 1.0 in Tunnels 16T, 11TWT, and 4T.

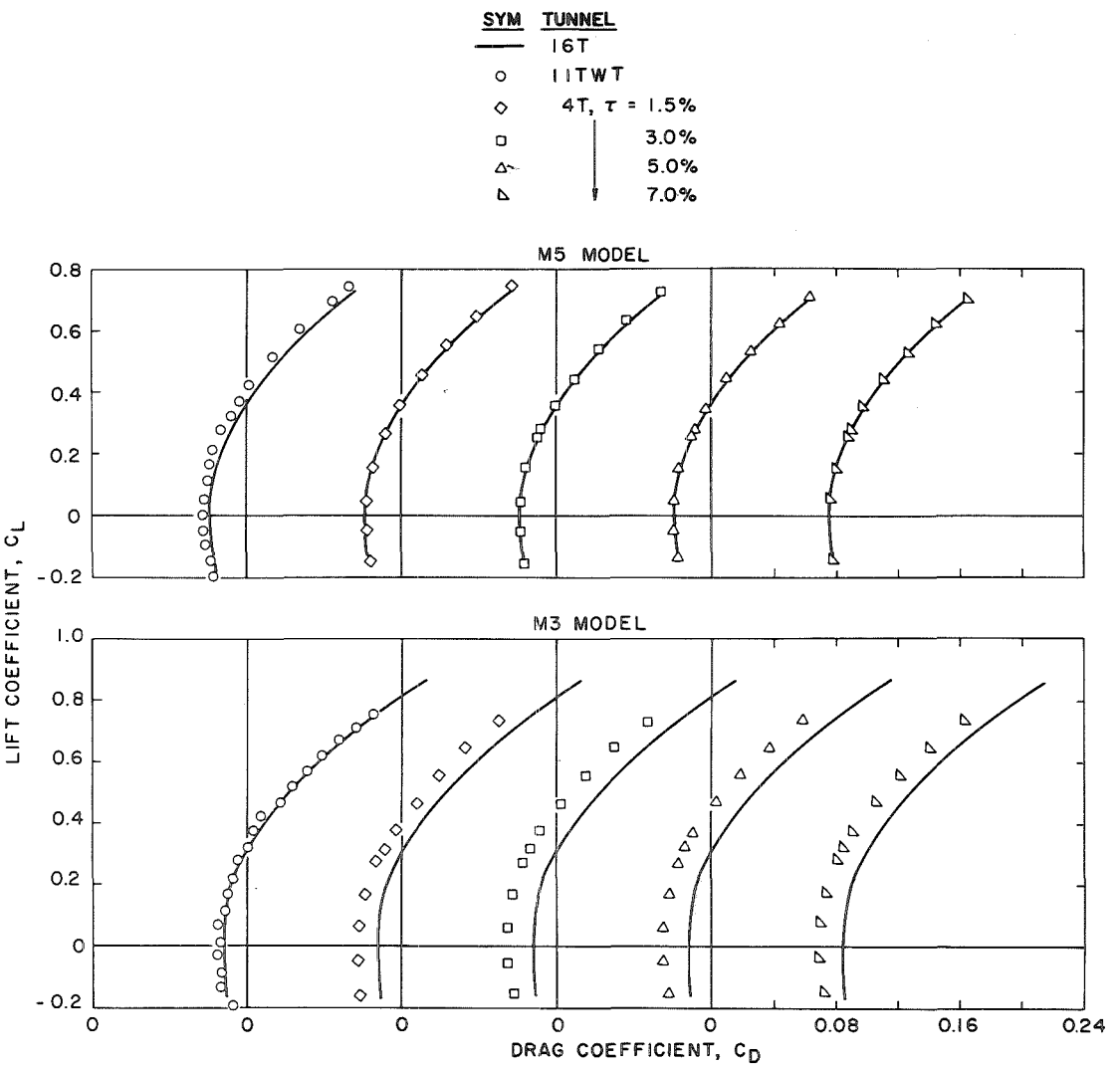

b. Drag coefficient
Figure 22. Continued.

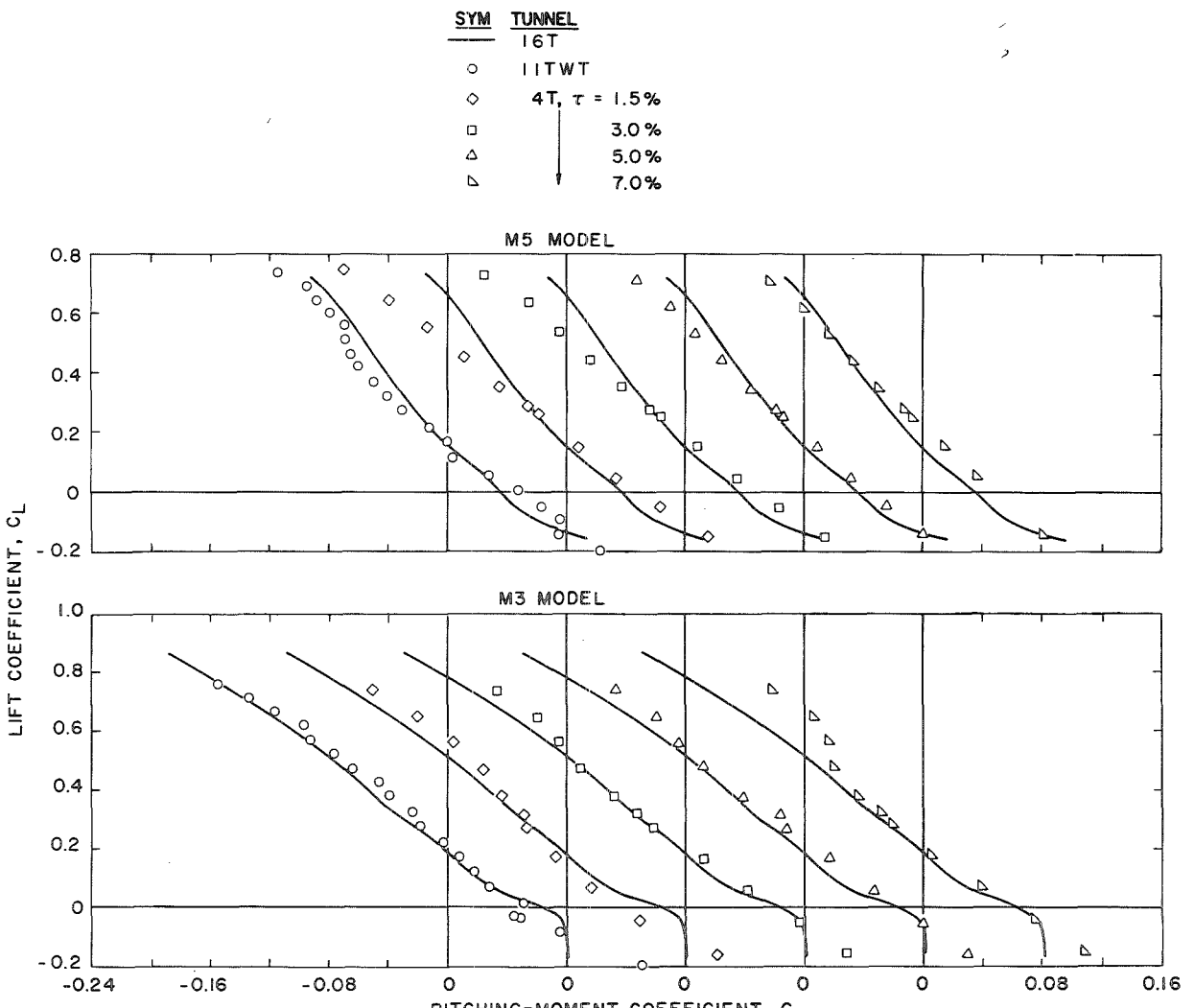

c. Pitching--moment coefficient
Figure 22. Concluded.

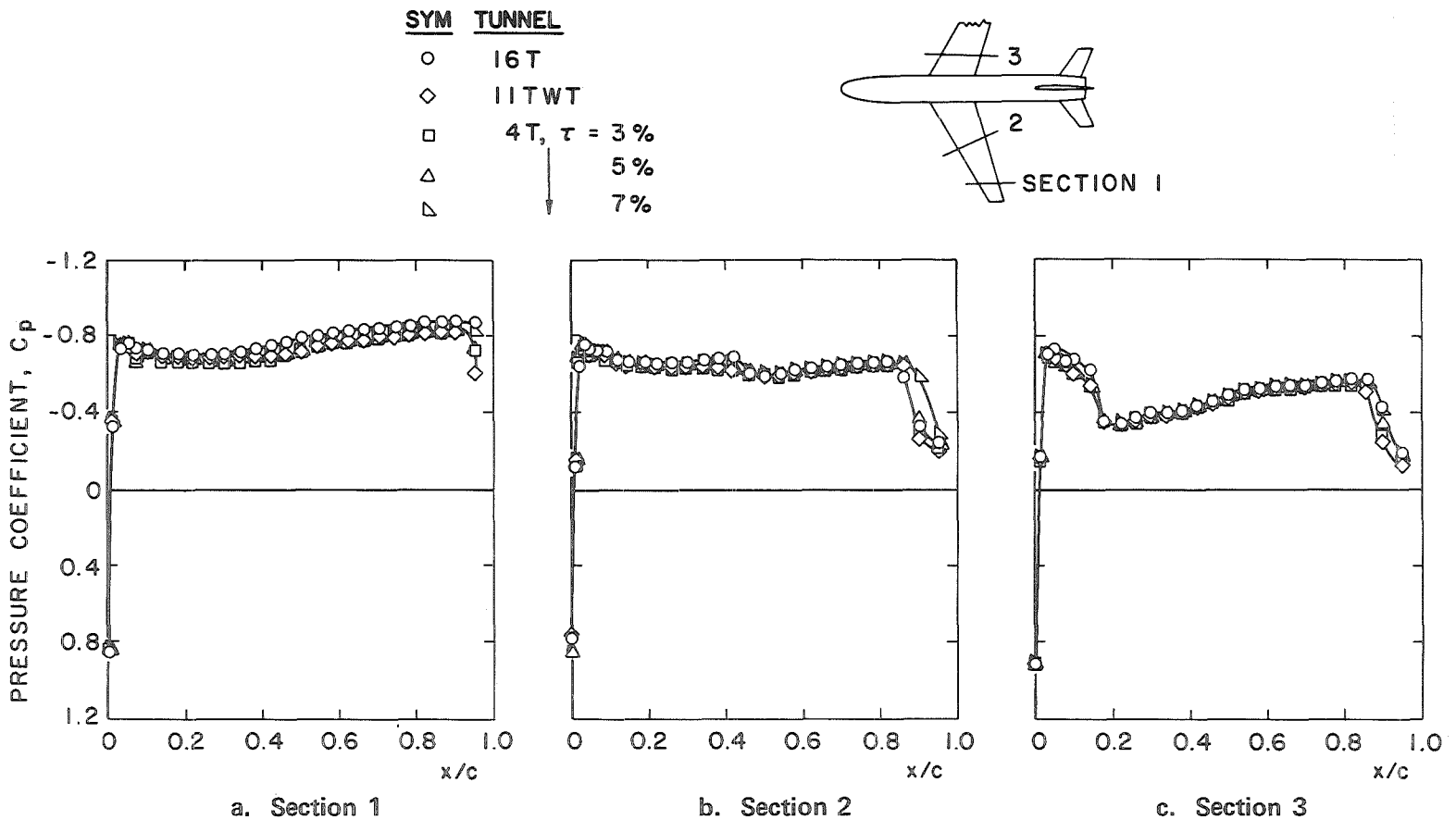

a. Section 1 b. Section 2 c. Section 3

Figure 23. Representative M5 wing pressure distribution at $M_\infty = 1.0$, $\alpha = 0.5$ deg.

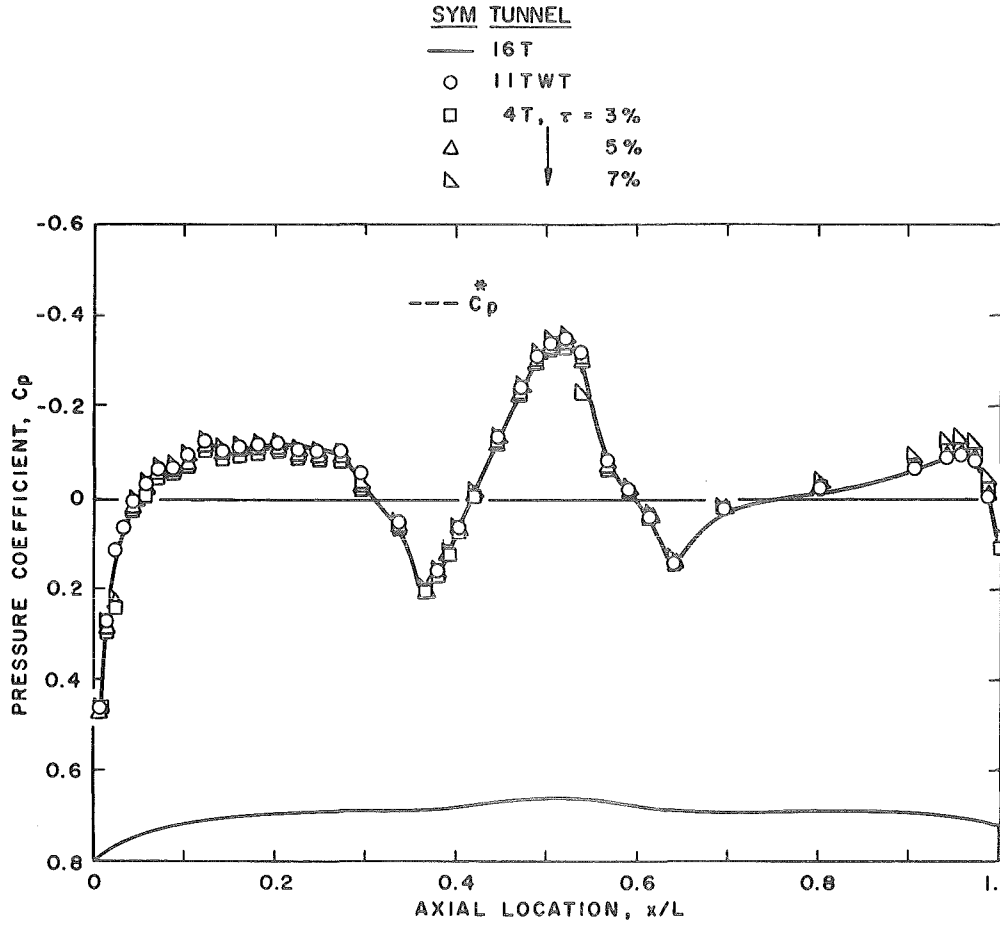

a. $M_\infty = 0.80$

Figure 24. Pressure distribution on the C5 model in three wind tunnels.

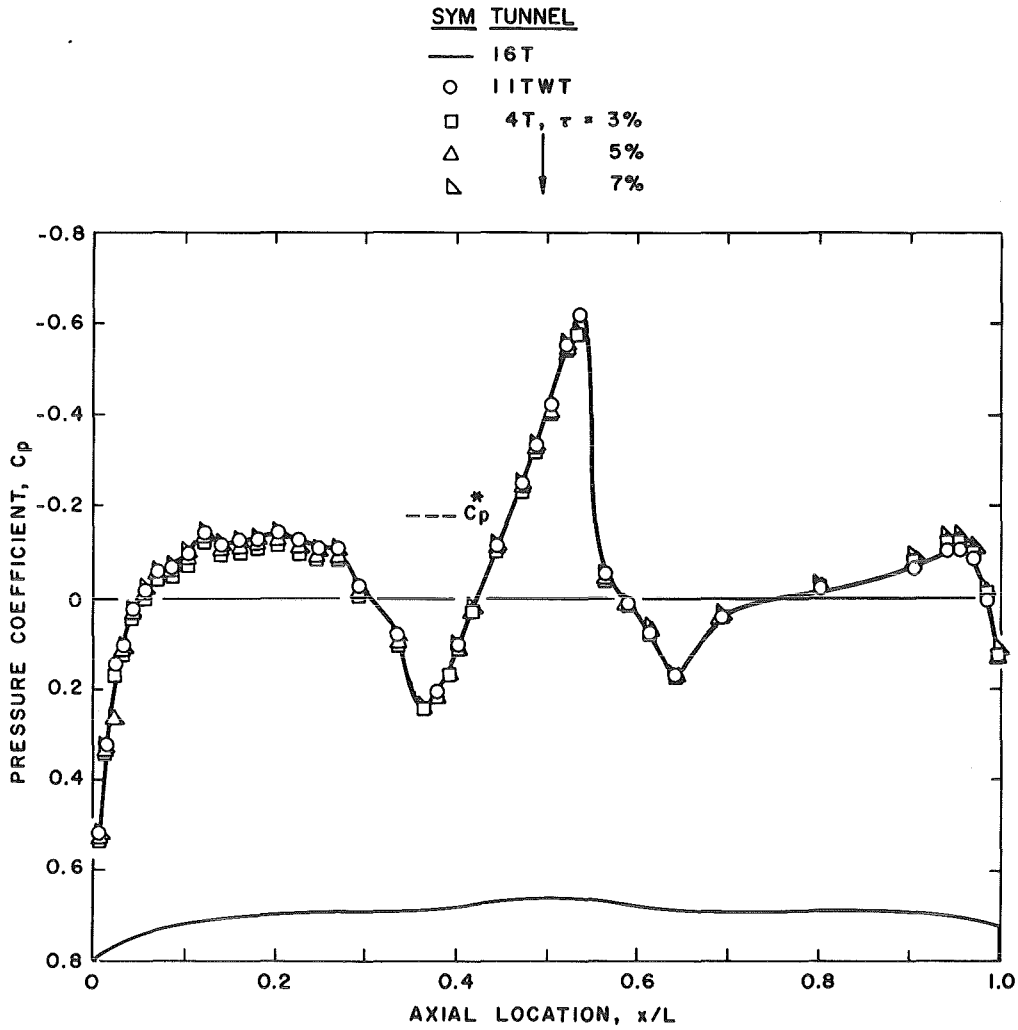

b. $M_\infty = 0.90$
Figure 24. Continued.

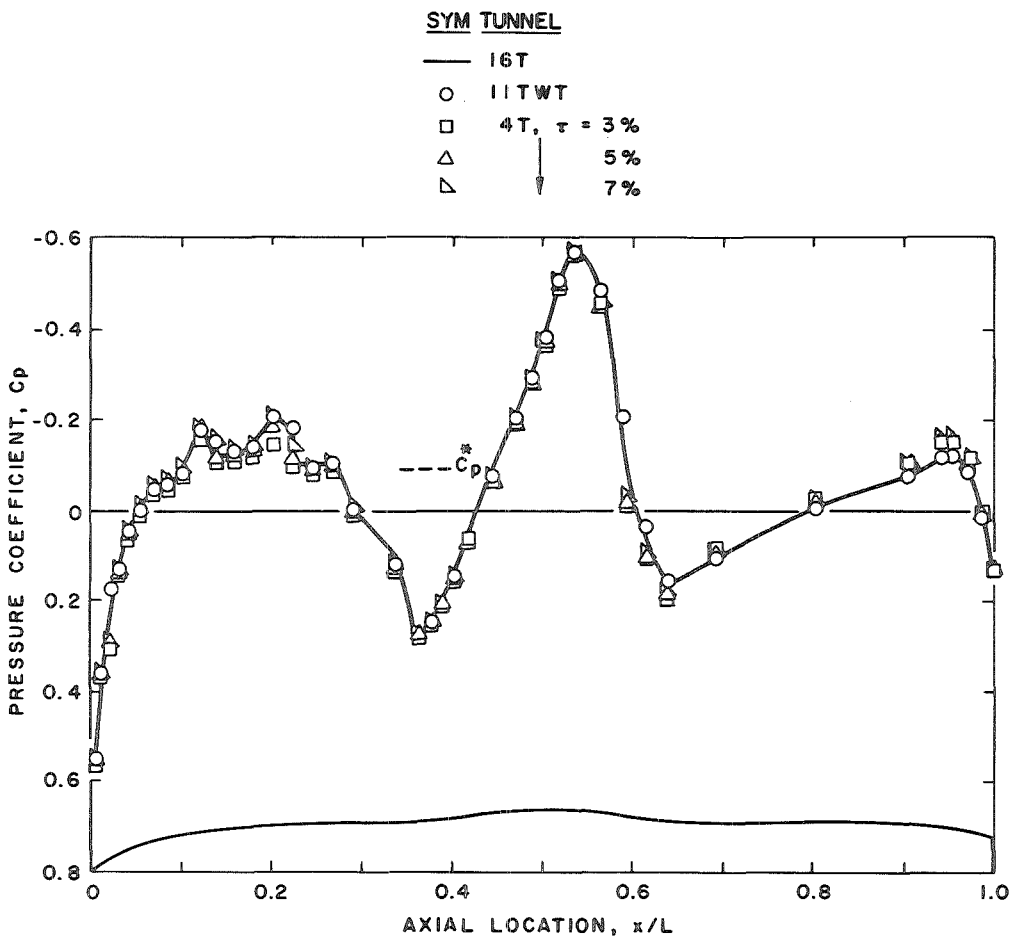

c. $M_\infty = 0.95$

Figure 24. Continued.

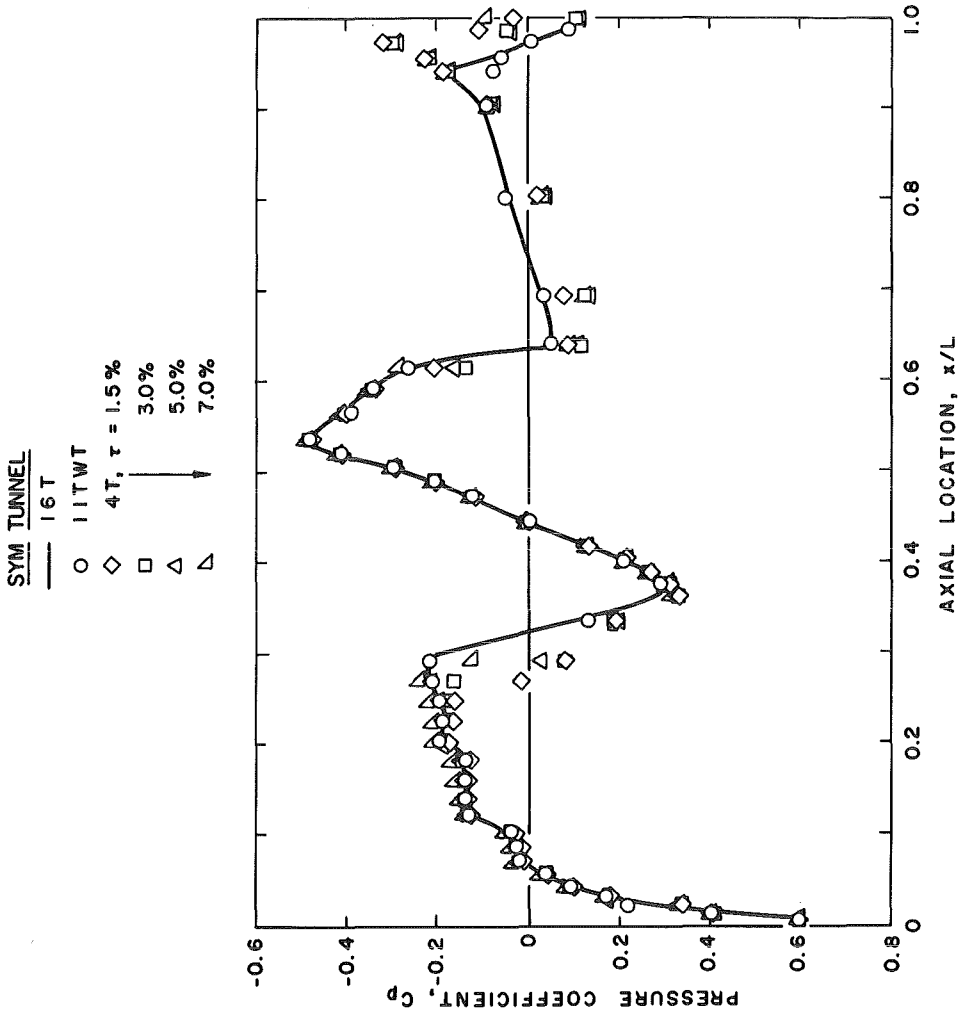

d. $M_\infty = 1.00$
Figure 24. Concluded.

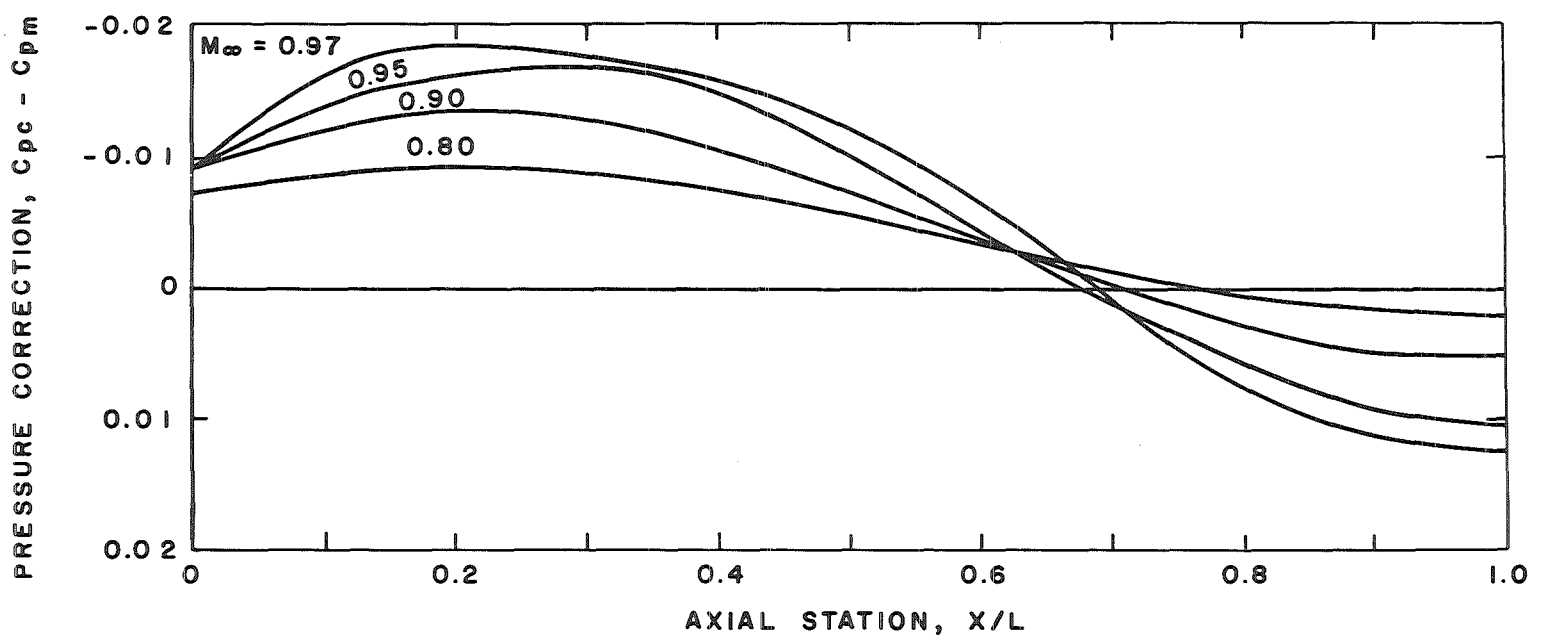

Figure 25. Theoretical blockage interference for the C5 model in Tunnel 4T, Q = 0.6.

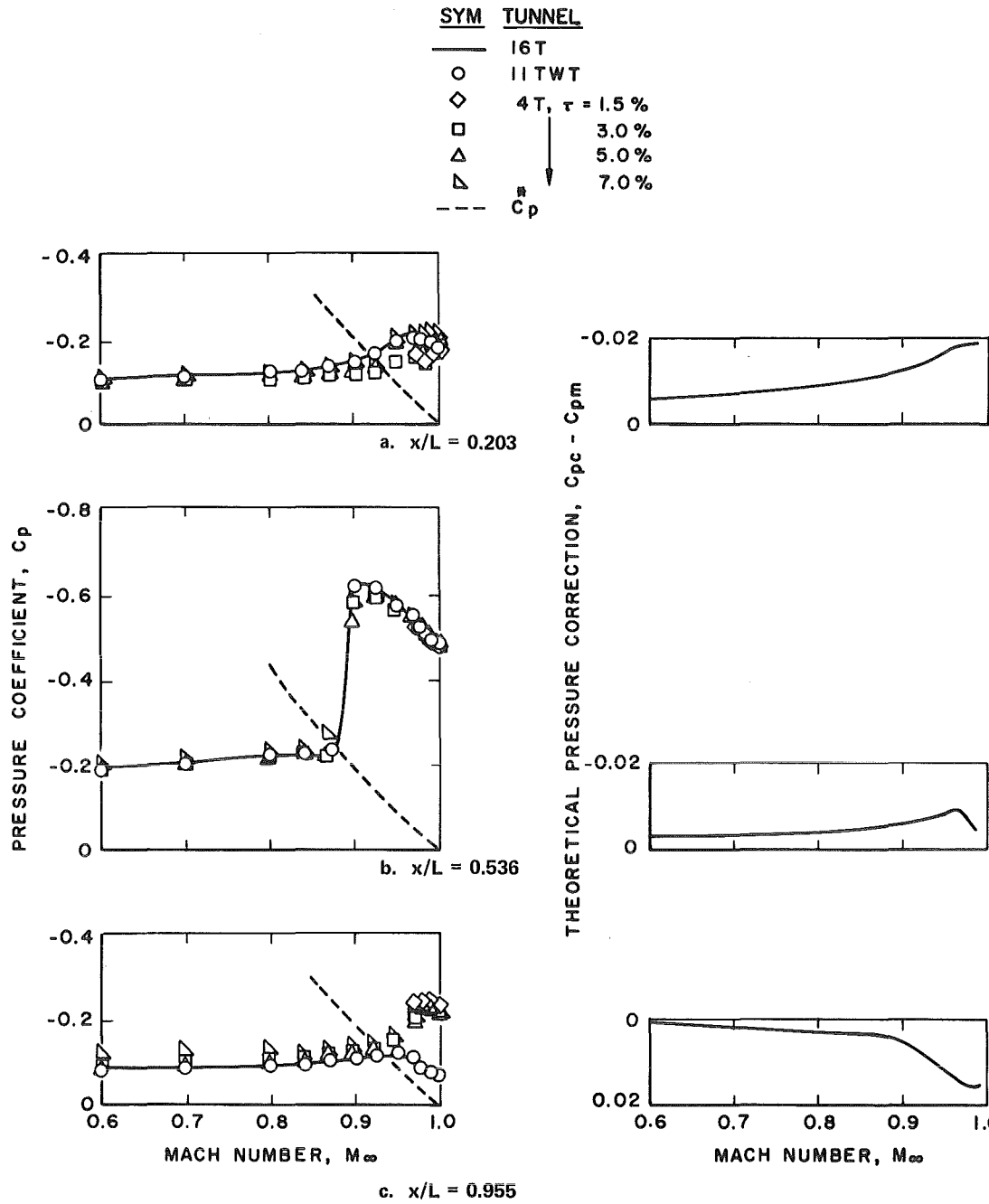

Figure 26. Effect of Mach numbers on local pressure measurements in the three wind tunnels, C5 model.

NOMENCLATURE

C_A	Axial-force coefficient
C_D	Drag coefficient
C_L	Lift coefficient
C_m	Pitching-moment coefficient
C_N	Normal-force coefficient
C_p	Pressure coefficient
C_p^*	Pressure coefficient at sonic velocity
C_{pc}	Pressure coefficient corrected for theoretical blockage interference
C_{pm}	Pressure coefficient from measured pressures
c	Wing chord, meters
L	C5 model length, meters
M_∞	Free-stream Mach number
P_{t_∞}	Free-stream total pressure
Q	Porosity parameter
Re	Reynolds number

x	Axial distance, meters
α	Angle of attack, deg
α_0	Angle of attack at zero lift, deg
τ	Tunnel wall porosity, percent